

TrafficGamer: Reliable and Flexible Traffic Simulation for Safety-Critical Scenarios with Game-Theoretic Oracles

Guanren Qiao¹, Guorui Quan², Jiawei Yu¹, Shujun Jia³, Guiliang Liu^{1*}

¹The Chinese University of Hong Kong, Shenzhen

²The University of Manchester

³Shenyang MXNavi Co.,Ltd.

*Corresponding Author, liuguiliang@cuhk.edu.cn

Abstract

While modern Autonomous Vehicle (AV) systems can develop reliable driving policies under regular traffic conditions, they frequently struggle with safety-critical traffic scenarios. This difficulty primarily arises from the rarity of such scenarios in driving datasets and the complexities associated with predictive modeling of multiple vehicles. The simulation of safety-critical traffic events that can support the testing and refinement of AV policies is an essential challenge to be addressed. In this paper, we introduce TrafficGamer, which facilitates game-theoretic traffic simulation by viewing common road driving as a multi-agent game. When we evaluate the empirical performance across various real-world datasets, TrafficGamer ensures both the *fidelity* and *exploitability* of the simulated scenarios, guaranteeing that they not only statically aligned with real-world traffic distribution but also efficiently capture equilibriums for representing safety-critical scenarios involving multiple agents. Additionally, the results demonstrate that TrafficGamer provides highly *flexible* simulations across various contexts. Specifically, we demonstrate that the generated scenarios can dynamically adapt to equilibriums of varying tightness by configuring risk-sensitive constraints during optimization. To the best of our knowledge, TrafficGamer is the first simulator capable of generating more realistic and adaptable traffic simulations based on the game-theoretic oracles, enhancing decision-making for autonomous agents and improving overall quality of safety-critical scenarios. We have provided a demo webpage for the project at: <https://qiaoguanren.github.io/trafficgamer-demo/>.

Introduction

As a cutting-edge technology, autonomous driving is a critical component of future transportation systems. The development of Autonomous Vehicles (AV) requires extensive testing and calibration of their control systems. Given the significant risks involved in conducting these tasks on real roads, the industry commonly relies on traffic simulation systems to ensure the safe development of AVs. Within these simulation systems, the commonly studied goals

include *traffic flow simulation* (e.g., SUMO [1] and CityFlow [2]), *sensory data simulation* (e.g., Airsim [3] and Unisim [4]), *driving policy simulation* (e.g., Highway-Env [5], SUMMIT [6], Metadrive [7], Commonroad [8], Intersim [9], Tbsim [10], Waymax [11], TorchDriveEnv [12] and CarDreameer [13]), *vehicle dynamics simulation* (e.g., Carsim [14] and Matlab [15]) and *multi-task simulation* (e.g., Carla [16], NVIDIA’s Drive Sim [17] and VI Worldsim [18]).

Major advancements made in traffic simulation have primarily focused on improving fidelity by replicating observed vehicle trajectories. While these methods can guarantee the expected accuracy of reproducing real-world traffic flows, they often fail to capture rare events that occur at the long-tail end of the data distribution. Conversely, a significant challenge in the design of modern AVs is their difficulty in managing these safety-critical "tail-end" events, rather than the more commonly observed traffic scenarios. This aspect underscores the importance of actively simulating safety-critical but infrequent events, which are crucial for thoroughly testing the reliability and robustness of AV control systems.

Beyond replicating realistic traffic scenarios, some recent studies have specifically focused on modeling safety-critical events. These event generating strategies can be categorized as follows [19]: (1) *Data-driven generation* detects and reproduces safety-critical scenarios recorded in real-world datasets. Some recent advancements, including Simnet [20], TrafficGen [21], Traffic-sim [22], VBD [23], NeuralNDE [24], Goal-LBP [25] and SceneGen [26], model the distribution of traffic scenarios by maximizing the likelihood of observed vehicle trajectories. (2) *Adversarial generation* intentionally creates risky scenarios by manipulating the generation process of autonomous vehicle (AV) systems [27]. Under this setting, Advsim [28] and STRIVE [29] manipulated the scenario’s initial conditions or provided the complete trajectory upfront. The Reinforcement learning (RL)-based methods constructed an adversarial policy network [30–32] to control autonomous vehicles. (3) *Knowledge-based generation* leverages external domain knowledge to facilitate the generation of safety-critical events. To apply this strategy, Robust-Traj [33], ChatScene[34], CGT [35], RTR [36] and GCRL [37] incorporated latent embeddings or constraint signals of traffic rules into their trajectory prediction models.

The aforementioned approaches primarily imitate human demonstrations and manually-crafted heuristics. However, as shown in Figure 1a, safety-critical traffic scenarios involve complex systems with multiple agents. These high-risk events are sparsely represented in real-world demonstration data, leading to higher predictive errors and crash rates in the imitation models. Such discrepancies impact the effectiveness of data imitation and human experience. More importantly, the agents’ behaviors in these systems are intricately interconnected and interdependent, and the reactions of one agent are largely dependent on the movements of others. Moreover, these reactions are shaped by the agents’ specific objectives and shared safety concerns, and referring only to log-reply is insufficient, as shown in Figure 1b. There is a lack of mechanisms that can effectively model the strategic behaviors of AV agents and actively formulate safety-critical events conditional on different environments.

To this end, a critical step toward achieving accurate strategic traffic simulations is to develop a game-theoretic traffic simulation algorithm designed to model the complex interactions among multiple agents in traffic scenarios. Such a system must be reactive, enabling vehicles to adapt to the movements of other traffic participants. From the perspective of game theory, whenever we modify the policy of a vehicle, the multi-agent system should converge to form a new equilibrium, from which no agent has an incentive to deviate. These characteristics would

provide advantages over simulators that primarily rely on imitation learning.

To ensure the practical application of these simulated strategic behaviors, it is essential to resolve the following challenges shown in Figure 1c: (1) *Distributional Fidelity*: The generated vehicle trajectories should closely replicate the behaviors of human drivers to provide realistic driving scenarios. Unlike imitation-based methods that focus on point-wise regression, the simulated scenarios should maintain a minimal distribution distance from the realistic dataset to ensure their alignment with naturalistic driving behaviors. (2) *Efficient Exploitability*: The algorithm simulates the competitive interactions among multiple agents. The algorithm should efficiently identify and converge to form an equilibrium, where no agent has an incentive to deviate. Furthermore, this process must be scalable to accommodate a large number and diverse types of vehicles. (3) *Flexible Simulation*: While an equilibrium typically assumes that the agents aim to maximize their expected returns, human drivers’ behaviors are inherently diverse and sensitive to various safety risks (i.e., bounded rationality). Maintaining an overly tight equilibrium may result in an inaccurate representation of drivers’ behaviors and limit the opportunities for controllers to develop safe policies. Therefore, it is crucial to control the tightness of the equilibrium. This advancement would offer the safety and flexibility needed for policy improvement and accommodate the nuanced and variable nature of human driving behaviors.

In response to the outlined challenges, we propose the use of TrafficGamer, a game-theoretic algorithm designed to facilitate distributional fidelity, efficient exploitability, and flexible simulation in multi-agent traffic simulations within complex environments. The overall framework of TrafficGamer is shown in Figure 2a. Specifically, TrafficGamer pre-trains a generative world model using large-scale traffic data collected from a variety of traffic scenarios. The pre-training is implemented through an end-to-end motion-prediction task that forecasts the future position of a vehicle based on historical observations of dynamic world features (e.g., surrounding vehicles) and state features (e.g., map attributes). This approach ensures that the traffic model accurately reflects, with high fidelity drivers’ preferences under realistic conditions. Subsequently, TrafficGamer fine-tunes this model by following a game-theoretic oracle. This refinement process involves minimizing the distributional distance to the pre-trained model, thereby maintaining the fidelity of the realistic data distribution while capturing the competitive behaviors among different AV agents. The AVs’ policies derived from our model can be mathematically characterized by a Coarse Correlated Equilibrium (CCE). We developed the multi-agent CCE-Solver algorithm to efficiently approximate this equilibrium, as shown in Figure 2b. The theoretical foundation for the optimality of our algorithm is grounded in recent advancements in a multi-agent CCE [38–40]. While the empirical performance of the algorithm draws upon principles from Magnetic Mirror Descent (MMD) [41–44]. This combination of theoretical and empirical insights ensures that our approach is robust and effective in complex traffic simulation scenarios. To dynamically adapt the tightness of the equilibrium, TrafficGamer incorporates a configurable safety constraint into its CCE policies (See Figure 2c). For example, by maintaining a larger distance between cars, we derive a softer CCE by implementing risk-preventing constraints. In this setting, agents are inclined to cooperate to meet joint safety constraints, such as maintaining appropriate distances between vehicles. This strategy ensures both safety and flexibility in traffic simulations.

As a scalable algorithm, TrafficGamer can be adapted to suit various datasets. To

demonstrate the scalability of TrafficGamer, we evaluate its empirical performance using well-known traffic datasets such as Argoverse 2 [45] and Waymo Open Motion Dataset [46], as well as a commonly used simulator. Specifically, we conduct three main sets of experiments and illustrate the results obtained under a variety of driving scenarios (12 in total): (1) *Fidelity Validation for the Generated Motion Trajectories*: We demonstrate that the trajectories generated by TrafficGamer can accurately characterize real-world traffic scenarios. Specifically, by quantifying the distributional divergence between generated traffic features (including distance between vehicles, speed, and collision rate) and those observed in the dataset, we show that the scenarios from TrafficGamer can statistically match the distribution of data from the real world. (2) *Efficient Exploitability under a Variety of Scenarios*: We illustrate that TrafficGamer can vary effectively close the Coarse Correlated Equilibrium Gap (CCE-Gap), thereby efficiently capturing the equilibrium necessary for representing safety-critical scenarios under a variety of traffic conditions. (3) *Simulation of Diverse Safety-Critical Scenarios*: To demonstrate the flexibility of its traffic simulations, TrafficGamer supports both 2D and 3D visualizations of each driving scenario from multiple perspectives. These visualizations show that TrafficGamer can generate a variety of intriguing and infrequent safety-critical traffic scenarios. Additionally, it can effectively configure the degree of competition and collaboration among vehicles within these scenarios. Illustrative videos are provided in the supplementary materials.

The impact of TrafficGamer is rooted in its capacity to generate reliable and flexible traffic scenarios that accurately reflect real-world safety-critical conditions, thereby enabling a more effective evaluation of autonomous driving systems. The primary objectives of TrafficGamer are to enhance the realism of traffic simulations, support robust decision-making for autonomous agents, and ultimately improve the comprehensive quality of safety-critical scenarios.

Results

Dataset

While real-world scenarios are crucial for the development and evaluation of autonomous vehicle (AV) systems, datasets of real-world for safety-critical scenarios are rarely available. Therefore, we assess the performance of our model using the publicly available dataset **Argoverse 2** [45], which contains 250,000 scenarios extracted from six distinct urban driving environments across the United States. **Argoverse 2** provides diverse and intriguing vehicle trajectories and environments for constructing autonomous driving systems. It has data for 10 diverse objects from dynamic and static categories including cars, buses, pedestrians, bicycles, etc. Each scenario is accompanied by a local vector map and 11 seconds (at a rate of 10 Hz) of trajectory data, detailing the 2D position, velocity, and orientation of all observed tracks relative to the ego vehicle’s perspective within the local environment. More details on the dataset can be found in Supplementary Section 1a.

Additionally, to demonstrate the robustness and generalization of our approach, we further evaluate our method using the **Waymo Open Motion Dataset** v1.2.0 [46]. This dataset features over 570 hours of unique data, covering 1,750 kilometers of roadways and over 100,000 scenes, each lasting 20 seconds and recorded at 10 Hz. It includes data on detailed interactions

between vehicles, pedestrians, and cyclists across six cities in the United States. More detailed information on this dataset is available in the Supplementary Section 1a.

Experimental Settings

Based on the trajectory prediction task setting, our generative world model predicts an agent’s future states by observing the agent’s historical information, map features, surroundings, and neighboring agents. By iteratively performing this prediction process, TrafficGamer teaches a CCE solver to generate traffic congestion scenarios with varying degrees of competition. To verify the generative performance of our algorithm, we select six representative scenarios from the validation datasets of Argoverse 2 and Waymo respectively, including (1) *Merge* where two separate lanes of traffic join into a single lane, (2) *Dual-lane intersection* where five cars with different destinations drive through a two-way intersection, (3) *T-junction* where one road ends at a perpendicular junction with another road, forming a "T" shape, (4) *Dense-lane intersection* where cars enter a four-way intersection with dense traffic. (5) *Roundabout* where traffic flows counterclockwise around a central circle, and (6) *Y-junction* where three directions of traffic flow converge at a single intersection. Figure 3 showcases the road map for our experiments in the last time step of the historical trajectories. In the training procedure, we utilize all training datasets to teach the generative world model. We then leverage validation datasets to evaluate our world model’s performance. In the fine-tuning stage, TrafficGamer controls 5-7 agents within the twelve scenarios selected from the validation datasets to simulate various safety-critical events by modeling different traffic congestion levels. More details about the experimental settings can be found in Supplementary Section 1b.

Evaluation Metrics

We leverage a comprehensive set of statistical metrics to evaluate the fidelity and effectiveness of the proposed TrafficGamer. The following metrics are included:

Fidelity. Fidelity metrics measure how well the simulated traffic distribution (i.e., the distribution of vehicles’ temporal and spatial features) matches the observed data distribution. We implement these fidelity metrics with *f-Divergence* $D_f(P||Q)$ which measures the divergence between two probability distributions P and Q over the space \mathcal{X} , so that:

$$D_{f_\alpha}(P||Q) \equiv \int_{\mathcal{X}} f \left(\frac{dP}{dQ} \right) dQ \quad (1)$$

where $f_\alpha : [0, +\infty) \rightarrow (-\infty, +\infty]$ denotes a convex function where $f(t)$ is finite for all $t > 0$, $f(1) = 0$, and $f(0) = \lim_{t \rightarrow 0^+} f(t)$. In this paper, we study the following implementation of D_{f_α} :

- By setting $f(t) = \frac{1}{2}(\sqrt{t} - 1)^2$, *f-Divergence* becomes *Hellinger distance* D_H such that:

$$D_H(P||Q) = \frac{1}{2} \int_{\mathcal{X}} \left(\sqrt{P(dx)} - \sqrt{Q(dx)} \right)^2 \quad (2)$$

- By implementing $f(t) = t \ln t$, f -Divergence can be transformed into *Kullback-Leibler divergence* (KL). We can calculate *KL-divergence* D_{KL} as:

$$D_{KL}(P\|Q) = \int_{\mathcal{X}} \left(P(dx) \log \frac{P(dx)}{Q(dx)} \right) \quad (3)$$

Additionally, as f -Divergence remains undefined when the support of the compared distributions is non-overlapping, our experiment includes the *Wasserstein Distance* of two probability distributions to avoid the appearance of inaccurate results. For a finite moment $p \in [1, +\infty]$, the Wasserstein p -distance between two probability distributions P and Q is defined by:

$$W_p(P, Q) = \inf_{\gamma \in \Gamma(P, Q)} \left(\mathbf{E}_{(\mu, \nu) \sim \gamma} d(\mu, \nu)^p \right)^{1/p}, \quad (4)$$

where $\Gamma(P, Q)$ is the set of couplings for distribution P and Q . Aiming at computational tractability, in our experiments, we set $p = 1$.

We demonstrate the fidelity of our method in modeling safety-critical events. A crucial metric that reflects the safety of simulated traffic is the *crash rate*. Supplementary Section 3c outlines the relevant details.

Exploitability. An exploitability metric reflects the optimality of the joint policies under a General Sum Markov Game (GS-MG)[47]. The traffic simulation reflects the optimality of simulated vehicles in quickly reaching their destinations under traffic rules and other constraints. This study characterizes this optimality by the CCE:

Definition 1. (ϵ -approximate CCE). A General Correlated policy π [48] is an ϵ -approximate Coarse Correlated Equilibrium (ϵ -CCE) if

$$\max_{i \in [I]} \left(V_{0,i}^{\dagger, \pi^{-i}}(s) - V_{0,i}^{\pi}(s) \right) \leq \epsilon \quad (5)$$

where $V_{0,i}^{\dagger, \pi^{-i}}(s) = \sup_{\pi'_i} V_{0,i}^{\pi'_i, \pi^{-i}}(s)$ denotes the best response for the i^{th} agent against π_{-i} . We say π is an (exact) CCE if the above is satisfied with $\epsilon = 0$.

Under this definition, a CCE-gap(i) = $V_{0,i}^{\dagger, \pi^{-i}}(s) - V_{0,i}^{\pi}(s)$ quantifies the deviation between the learned policies of each agent and the performance of the best equilibrium policy. In our study, $V_{0,i}^{\pi}(s) = V_{0,i}^{\pi, r}(s) + \lambda V_{0,i}^{\pi, c}(s)$, where r is denoted as the reward and c is the cost. Unlike the Nash Equilibrium (NE) [49] which enforces the independence of each agent during optimization, a CCE permits interdependencies among the agents' policies, allowing each agent's strategy to be informed by the strategies of others. We assess the CCE-gap, as it better aligns with the decision-making processes of human drivers, who typically base their actions on the behaviors of nearby vehicles. Additionally, it simplifies the challenge of convergence, as CCEs are inherently less restrictive and more prevalent than NEs.

We compare the proposed method with QCNet [50], Multi-Agent Proximal Policy Optimization (MAPPO) [51], and GameFormer [52]. QCNet jointly predicts the trajectory of multiple agents under a supervised learning framework. MAPPO is a policy gradient algorithm designed for multi-agent reinforcement learning (MARL). GameFormer proposes a game-theoretic model and learning framework for interactive prediction and planning using Transformers. More details on the baselines can be found in Supplementary Section 1c.

Fidelity Validation of Generated Motion Trajectories

A crucial prerequisite for a safety-critical traffic simulation is that it aligns with realistic traffic scenarios. We characterize this alignment with distributional fidelity (see Evaluation Metrics section), which quantifies the divergence between realistic traffic distributions and those simulated by our TrafficGamer. Among the spatial and temporal traffic features, vehicle speed, and inter-vehicle distance are the most commonly used features for examining the performance of AV simulators [24]. We adapt f -divergence to qualify how well the simulated distributions of vehicle speed and car distance match the realistic ones from the large-scale traffic datasets (Argoverse 2 and Waymo).

In this experiment, we assess fidelity by quantifying the distributional divergence using several divergence metrics, including the Kullback-Leibler divergence, Hellinger distance, and Wasserstein distance [53] (Figure 4). We find the experiment results, and we find the simulated scenarios generated by our TrafficGamer can properly imitate the real-world distribution of instantaneous vehicle speeds and vehicle distances. Specifically, for methods based on *multi-agent fine-tuning* (TrafficGamer and MAPPO), we observe a smaller divergence between realistic traffic data and the simulated traffic features generated by TrafficGamer is smaller compared to those produced by MAPPO. This is because the MMD objective in our TrafficGamer (Objective 12) explicitly minimizes the divergence from the observed policy during optimization. The reduction in divergence results in a more accurate replication of vehicle speed and distance distributions, indicating that the learned multi-agent policies are more closely aligned with actual human driving behaviors. Moreover, the performance of TrafficGamer is comparable to that of imitation learning-based methods (QCNNet and GameFormer) in terms of ensuring the fidelity of realistic driving behaviors.

To better evaluate our method’s effectiveness in replicating humans’ driving styles across various scenarios, we categorize the scenarios into specific types, including *fork road* and *cross road*. We then compare the learned and actual distributions of distance and speed (Figure 4, rows from 3 to 6). In the crossroad scenario (rows 5 and 6 in Figure 4), TrafficGamer’s performance is comparable to, albeit slightly less robust than, that of QCNNet in maintaining fidelity. This result is as anticipated, as QCNNet is designed to closely mimic the observed behaviors of drivers, resulting in trajectories that heavily overlap with those in the source dataset. Another key observation is that our method, TrafficGamer, significantly outperforms standard MARL approaches such as MAPPO. This demonstrates TrafficGamer’s capability in accurately replicating a wide range of human driving behaviors and generating realistic driving scenarios. We also checked the fidelity of TrafficGamer for the Waymo motion dataset, and the results closely match the ground-truth distribution. More details can be found in Supplementary Section 3d.

Efficient Exploitability Under a Variety of Scenarios

Standard RL algorithms focus on reward maximization; however, in the multi-agent autonomous driving environment, we primarily consider exploitability [43], which measures the extent to which a vehicle’s policy can exploit the current traffic policies. An ideal driving equilibrium should have zero exploitability, meaning no single vehicle can achieve greater benefits by continually improving the policy. In this paper, we follow the methodology outlined in [47] and

utilize the **CCE-gap** (see Definition 1) to measure exploitability. Unlike the commonly studied toy environments (e.g., Bargaining, TradeComm, and Battleship [44]), the traffic scenarios involve complex game contexts, multiple agents, and continuous action space, which makes the best response π_i^\dagger computationally intractable, thus accurately calculating the exact CCE-gap becomes challenging. Therefore, we estimate the CCE-gap by empirically approximating π_i^\dagger via the following methods:

- *Breaking the Equilibrium.* Upon the convergence of the studied algorithm converges, we estimate each agent’s best response under the current equilibrium, denoted as π_i^\dagger , by fixing the policies of the other $I - 1$ agents and continuously encouraging this agent to maximize its current reward. This process assesses the agent’s ability to disrupt the existing equilibrium. If none of the policies can achieve significantly higher rewards, it indicates that the experimental algorithm has successfully identified a reliable CCE.
- *Restricting Action Space.* To overcome the computational intractability caused by complex driving behaviors, we constrain the choice of the decision-making domain to choose actions from a predefined candidate set. This set is generated via a pre-trained action predictor (see Objective 9), which identifies and ranks the top K actions most similar to those observed in the dataset. Within this tractable action space, we compute π_i^\dagger by selecting the actions that optimally maximize rewards at each step.

We compare the performance of TrafficGamer in all Argoverse 2 scenarios with other baselines based on the aforementioned CCE-Gaps. The CCE-gaps achieved for each agent during training are presented in Figure 5 and Figure 6. The training curves of QCNet and GameFormer show their performance is unstable and they struggle to converge at the CCE. The results illustrates that end-to-end imitation learning methods can not model competitiveness between agents, which makes it difficult to optimize policies for capturing the CCE. MAPPO performs better than other baselines, but it falls short of the results obtained by TrafficGamer. MAPPO faces challenges in efficiently exploring the entire policy space of the multi-agent game environment during the optimization process, making it difficult to capture the underlying CCE. As a solver defined for CCE, TrafficGamer ensures that the agents’ policies are distributionally aligned with human-driven policies and supports stable exploration. This allows each agent to learn the optimal policy and gradually converge to an approximate CCE.

The CCE-gap of each agent at the end of the training is presented in Table 1 and Table 2¹. TrafficGamer achieves a smaller CCE-gap than other methods, demonstrating its superior exploitability across various scenarios. However, it exhibits slightly lower performance for certain agents in some scenarios. An in-depth analysis reveals the two main reasons for this phenomenon: (1) TrafficGamer may struggle to effectively adapt to rapid changes in opponents’ strategies under specific conditions. For example, when surrounding vehicles accelerate, a particular vehicle may need to decelerate to maintain safe spacing. (2) Other vehicles’ presence significantly influences algorithm-controlled vehicles’ decision-making processes. For example, if a car on the other hand begins to merge into the current lane, the algorithm might adopt a more conservative driving strategy to prioritize safety, thereby influencing exploiting. Overall,

¹We calculate the mean \pm std of the CCE-gap, based on an average of over 300 episodes. The best average performance is highlighted in bold. N/A indicates this agent does not exist in this scenario.

in a multi-agent game environment, it is essential to evaluate the collective performance of all agents. TrafficGamer is capable of learning a CCE that approximates the optimal solution, resulting in more comprehensive modeling of vehicle-driving behaviors.

Simulation of Diverse Safety-Critical Scenarios

To demonstrate the ability of TrafficGamer to generate diverse traffic scenarios, we can visualize the generated scenarios with varying degrees of competitive behavior. Automated driving scenarios involve complex elements including road structures, traffic regulations, and vehicle behaviors, which can be challenging to interpret directly from raw data. To address this, we simulate the actual behavior of vehicles in various safety-critical scenarios and traffic conditions using 2D and 3D visualizations. These are captured in third-person and first-person views, to provide a clearer understanding of the dynamics at play. To facilitate 2D visualization, TrafficGamer supports the display of lines, markers, the road network, vehicle positions, and movement trajectories on a unified 2D plane by following the formats established for Argoverse 2 [45] and Waymo [46]. This approach uses concise symbols to represent various traffic elements, enhancing the intuitiveness of scene analysis. To capture the real-world complexity of traffic behaviors more accurately, TrafficGamer enables large-scale 3D traffic scenario modeling and simulation through **ScenarioNet** [54], based on the MetaDrive simulator [7]. The scenarios generated can be replayed and interactively explored from multiple perspectives, ranging from Bird’s Eye View layouts to realistic 3D renderings in ScenarioNet.

In this experiment, we explore how well TrafficGamer can generate different safety-critical scenarios under 12 distinct traffic scenarios. To generate diverse traffic scenarios, we design a constrained and risk-sensitive policy optimization method [55, 56] for capturing the equilibrium subject to different levels of tightness. Specifically, by adjusting the inter-vehicle distance constraints and risk coefficients, we derive a diverse number of traffic scenarios under different game contexts. Figure 7 illustrates the details of our results.

By comparing the scenarios generated with different levels of inter-vehicle distance constraints (from top to bottom in Figure 7 and Figure 8) , we find that, as the inter-vehicle distance increases, our model adapts, leading to traffic scenarios characterized by less competitive behavior and safer navigation across all examined situations. This outcome arises because maintaining distance constraints requires the cooperation of multiple vehicles. Imposing more restrictive constraints (i.e., increasing the distance) significantly enhances the impact of this cooperation on the optimization of Objective 16 (dynamically controlled by the Lagrange parameter λ). Figure 9 displays the variation in the Lagrangian penalty factor during the training process. As the constraints become tighter, the Lagrangian penalty term also increases, indicating that it has a larger impact on Objective 16. On the other hand, when we reduce the required distance, agents begin to prioritize their interests, which significantly increases the likelihood of traffic congestion where no agent can further optimize their policy. All these dynamic scenarios are characterized by the learned CCEs.

Similarly, by comparing the scenarios generated with different levels of risk sensitivity (from left to right in Figure 7), we find that imposing a higher confidence level leads to more conservative and cautious driving behaviors. A higher confidence level forces the agent to satisfy the constraints with greater probability, resulting in driving strategies that feature lower

speeds, increased spacing between vehicles, and more careful navigation through complex traffic scenarios. On the other hand, setting a lower confidence level results in more aggressive and risk-seeking driving behaviors, characterized by faster vehicle speeds and shorter following distances. The system’s tolerance for some aggressive behaviors (such as overtaking etc.) also increases. This approach can lead to a higher risk of collisions and increase the likelihood of critical safety scenarios in traffic.

These diverse scenarios are crucial for investigating the trade-offs between aggressive and conservative driving behaviors. By analyzing AV policies within these scenarios, we can more effectively evaluate the optimality of driving strategies across different levels of competition and congestion. Furthermore, the comprehensive 2D and 3D simulations provided by our TrafficGamer from both the third-person and first-person perspectives offer a detailed understanding of traffic dynamics. These simulations demonstrate how variations in risk sensitivity and distance constraints impact vehicle behavior in real-world driving scenarios.

Discussion

We have demonstrated that our model, TrafficGamer, can effectively represent various safety-critical traffic scenarios by capturing a range of CCEs. To the best of our knowledge, this is the first algorithm able to fine-tune generative world models to accurately model competitive and collaborative behaviors among multiple agents across various degrees of constraints and dynamic environments. Most importantly, TrafficGamer can accurately characterize traffic congestion scenarios that are frequently observed in reality but are underrepresented in datasets, such as roundabouts, intersections, and merge points. This capability ensures the high fidelity of TrafficGamer in simulating real-world applications.

To facilitate the reliable generation of our safety-critical scenarios, we resolved three critical challenges, including (1) how to guarantee the fidelity of generated trajectories, (2) how to efficiently capture the CCE of each scenario by modeling the competition behaviors of vehicles, and (3) how to dynamically adapt the strength of the equilibrium. These safety-critical scenarios can serve as important testbeds for AV when evaluating the reliability and robustness of AV-control algorithms before their practical deployment. Traditional simulation systems have relied heavily on manually designed rules or data-driven trajectory imitation, often resulting in scenarios that lack fidelity and diversity. Our model, TrafficGamer, addresses these limitations by generating a variety of realistic, safety-critical scenarios. It is important to note that our method currently models vehicle behaviors on a static map. Future enhancements for TrafficGamer may include the integration of multi-modal large models to generate scenarios that incorporate variations in vehicle behaviors in response to environmental factors, such as weather conditions, the time of day, and topography.

Methods

Problem Formulation

We formulate the task of multi-vehicle motion prediction in the traffic scenarios as a **Decentralized Partially Observable Constrained Markov Decision Process (Dec-POCMDP)**. $(\mathcal{S}, \{\Omega_i, \mathcal{A}_i, \mathcal{O}_i, r_i, c_i\}_{i=1}^I, \mathcal{T}, \gamma, p_0)$ where:

- i denotes the number of agents from 1 to I .
- Ω_i and \mathcal{A}_i denote the spaces of observations and actions for a specific agent i . The observations include the position, velocity, heading, and partial map features in the surrounding neighbor region of the agent i . The actions consist of relative heading and acceleration, as described in [11].
- \mathcal{S} denotes the state space that comprises all agents’ historical trajectory information and map features.
- $\mathcal{O}_i : \mathcal{S} \rightarrow \Omega_i$ denotes the observation function that maps states and actions to local observation for the i^{th} agent. $\mathcal{O} = \{\mathcal{O}_1, \dots, \mathcal{O}_I\}$ denotes the function set.
- $r_i : \{\Omega_i \times \mathcal{A}_i\}_{i=1}^I \rightarrow \mathbb{R}$ denotes the agent-specific reward function that maps actions and observations from all agents to the reward of i^{th} agent. We considered reward factors such as collision avoidance, lane deviation, and reaching the destination, etc.
- $c_i : \{\Omega_i \times \mathcal{A}_i\}_{i=1}^I \rightarrow \mathbb{R}$ denotes the agent-specific cost function that maps actions and observations from all agents to the cost of i^{th} agent. We adapt vehicle distance as a constraint condition, additionally, the expectation of cumulative constraint functions c_i must not exceed associated the thresholds episodic constraint threshold δ .
- $\mathcal{T} : \mathcal{S} \times \mathcal{A} \rightarrow \Delta^{\mathcal{S}}$ denotes the transition function.
- $\gamma \in [0, 1]$ and $p_0 \in \Delta^{\mathcal{S}}$ denote the discount factor and the initial distribution, respectively.

More details of reward and cost functions can be found in Supplementary Section 2a.

In the framework of Dec-POCMDP, each agent is assigned an individual reward function and cost function, denoted as $r_i(\cdot)$ and $c_i(\cdot)$. This aligns with a general-sum game structure [57], which is more complex and less explored than zero-sum and cooperative games [58, 59]. Figure 10 displays the differences between these three settings. Despite the challenges, modeling a general-sum game better aligns with real-world driving scenarios as human drivers often prioritize their objects. These objects can be applied to satisfy conflicting interests among different AV agents. During the optimization process, human drivers’ behaviors inevitably affect others’ decisions. Accordingly, we consider the **General Sum Markov Games (GS-MGs)** under the Dec-POCMDP. For the agent i , the value function $V_{i,t}^{\pi,r} : \mathcal{S} \rightarrow \mathbb{R}$, action-value

² $\Delta^{\mathcal{S}}$ denotes the probability simplex over the space \mathcal{S} .

function $Q_{i,t}^{\pi,r} : \mathcal{S} \times \mathcal{A}_i \rightarrow \mathbb{R}$ and advantage function $A_{i,t}^{\pi,r} : \mathcal{S} \times \mathcal{A}_i \rightarrow \mathbb{R}$ are represented by:

$$V_{i,0}^{\pi,r}(s) = \mathbb{E}_{p_0, \mathcal{T}, \pi} \left[\sum_{t=0}^T \gamma^t r_i(o_t, a_t) \mid \mathbf{o}_0 = \mathcal{O}(s_{t+1}) \right] \quad (6)$$

$$Q_{i,0}^{\pi,r}(s, a_i, -\mathbf{a}_i) = \mathbb{E}_{p_0, \mathcal{T}, \pi} \left[\sum_{t=0}^T \gamma^t r_i(\mathbf{o}_t, \mathbf{a}_t) \mid \mathbf{o}_0 = \mathcal{O}(s_{t+1}), a_{i,0} = a_i \right] \quad (7)$$

$$A_{i,0}^{\pi,r}(s, a_i, -\mathbf{a}_i) = Q_{i,0}^{\pi,r}(s, a_i, -\mathbf{a}_i) - V_{i,0}^{\pi,r}(s) \quad (8)$$

where $-\mathbf{a}_i = \{\mathbb{1}_{i' \neq i} a_{i'}\}_{i'=1}^I$ ³ denotes the joint action performed by $I - 1$ players (without i 'th player) and $\boldsymbol{\pi} = \{\pi_i\}_{i=1}^I$ denotes the product policy.

Under a GS-MG, the goal of policy optimization is capturing a **Coarse Correlated Equilibrium (CCE)** (Definition 1), which allows agents' policies to be interdependent, contrasting with NE where each agent optimizes independently. Unlike previous GS-MG policies [38, 40] that use the Markov policy $\pi_i(a|s)$, our method incorporates historical information, including the actions and observations of neighboring agents, to better characterize the decision-making process of AVs.

Unlike previous GS-MG solvers [39, 40, 57, 60, 61] that rely on an interactive environment, traffic simulation presents additional challenges, as our algorithm can only utilize an offline database with records of the behaviors of multiple drivers on open roads. Additionally, we incorporate constraints into the optimization process to allow the algorithm to learn the agents' behavior under traffic rules. This problem can be formulated as **Offline Multi-agent Constrained Reinforcement Learning (Offline MA-CRL)**. Using the offline database with records of the behaviors of multiple drivers on open roads, our algorithm aims to learn the CCE policies of multiple AVs under various constraints that accurately reflect the human drivers' behaviors in the dataset. Specifically, the problem can be summarized as follows:

Definition 2. (*Offline MA-CRL in GS-MGs.*) let $\mathcal{D}_o = \{\mathcal{M}_n, \tau_{n,1}, \dots, \tau_{n,I}\}_{n=1}^N$ defines the offline dataset, where $n = [N]$ defines the number of scenarios, \mathcal{M}_n represents the game context in the n^{th} scenario, $\mathbf{c} = \{c_0, c_1, \dots, c_i\}_{i=1}^I$ represents constraints and $\tau_{n,i} = \{o_{i,0}, a_{i,0}, \dots, o_{i,T}, a_{i,T}\}$ denotes the trajectory of i^{th} agent in the n^{th} scenario. Given \mathcal{D}_o , the goal of our algorithm is to learn a $\hat{\boldsymbol{\pi}}_{\mathbf{c}}$ that satisfies the constraints with the following properties: (1) *Exploitability*: $\hat{\boldsymbol{\pi}}_{\mathbf{c}}$ satisfies the ϵ -approximate CCE in Definition 1, and (2) *Fidelity*: $\hat{\boldsymbol{\pi}}_{\mathbf{c}}$ must be consistent with the real driver's policies such that $D_f(\hat{\boldsymbol{\pi}}_{\mathbf{c}}, \boldsymbol{\pi}^o) \leq \xi$ where D_f and ξ denote the divergence metric and a threshold, respectively.

In this work, to solve the offline MA-CRL problem in GS-MGs under the Dec-POCMDP (Definition 2), we consider a model-based MA-CRL approach that (1) **trains a generative world model** to acquire AV environment features in a data-driven way, (2) **converges to CCEs** based on the predicted environment dynamics and predefined action space and (3) adjusts the level of competition for **capturing diverse degrees of CCEs**.

³Throughout this work, the bold symbols (e.g., \mathbf{a}) indicate a vector of variables, while the non-bold ones (e.g., a) represent a single variable.

Modelling Traffic Dynamics Based on Offline Data

To represent the environmental dynamics, we introduce the generative world model, action predictor, and observation model based on the offline datasets D_l .

Generative World Model. For computation efficiency, we follow the decoder-only architecture in GPT [62] and implement the world model as an *Auto-regressive Trajectory Decoder*. As a sequential prediction model, our world model maps the previous state (e.g., s_{t-1}) and the action of each agent (e.g., $a_{1,t}, \dots, a_{i,t}$) onto the next state s_t . Unlike QCNet [50], which generates trajectories for future vehicle motions over a fixed period, our world model adopts an auto-regressive approach, predicting vehicles’ step-wise motion based on its previous predictions. This approach enables the modeling of how past movements influence future decisions.

Under the context of Dec-POCMDP, when $t = 0$, s_0 captures the static game map \mathcal{M} and initial features of all agents. when $t > 0$, $s_t = \{z_{i,w}^A\}_{w=t-W,i=0}^{t,I}$ captures the spatial-temporal information of all agents under the game map \mathcal{M} in the previous $t-1$ time steps, and $a_{1,t}, \dots, a_{i,t}$ denotes the acceleration and heading of agents in the current time step. Under this setting, our decoder is implemented by (1) *Agent-to-Map Cross Attention*, (2) *Agent-to-Temporal Cross Attention*, (3) *Agent-to-Neighbor Cross Attention* and (4) *Self-Agent Attention*, which incorporates map information, historical information, the spatial-temporal features of the surrounding agents, and the features of the agent itself into the temporal dimension thereby mapping s_t and $\mathbf{a}_{1,\dots,I,t}$ to s_{t+1} . The details of the implementation are illustrated in Figure 11. In addition, our world model also includes two other important modules:

Action Predictor. The actor model predicts the actions (acceleration and heading) based on the state $s_t = \{z_{i,w}^s\}_{w=t-W,i=0}^{t,I}$ to satisfy latent traffic rules in the realistic driving scenarios. The actor model $\pi_{i,t}(a_{i,t}|o_{i,t})$ denotes the probability of that i ’s agent generates an action a_t such that $\max_k \omega_i^k p(a_t|\mu_{i,t}^k, b_{i,t}^k) = \pi_{i,t}(a_{i,t}|o_{i,t})$ where (1) ω_i^k denotes a learnable coefficient and (2) p_k denotes the k -th mixture component’s Laplace density. We constrain the output actions within a reasonable range to prevent irrational driving behaviors such as sudden acceleration or deceleration, sharp turns, etc. In the subsequent RL fine-tuning stage, we sample the i -th agent’s future trajectory as a weighted mixture of Laplace distributions by following [50, 63]:

$$\pi^l(\hat{\tau}) = \prod_{t=1}^{\mathcal{T}} \pi_{i,t}^l(\hat{a}_{i,t} | o_{i,t}) = \prod_{t=1}^{\mathcal{T}} \sum_{k=1}^K \omega_i^k p(\hat{a}_{i,t} | \mu_{i,t}^k, b_{i,t}^k) \quad (9)$$

where ω_i^k can effectively act as the weighting coefficients and $\mu_{i,t}^k$ and $b_{i,t}^k$ characterize the mean position and the level of uncertainty, respectively, of the i -th agent at the time step t .

Observation Model For each agent, our observation model maps s_t and $a_{i,t}$ onto agent-specific observations $\{o_{i,t}\}_i^I$. The observation model is implemented by $o_{i,t} = f_i^{\text{MLP}}(z_{i,t}^A)$, where MLP is the Multilayer Perception. Additionally, this module considers the historical actions and observation of all agents such that $\mathbf{h} = \{(o_{i,t}, a_{i,t})\}_{t=0,i=1}^{w,I}$.

Recognizing CCEs in the General Sum Markov Games

As our environment is structured as a multi-player competitive game with rewards and costs specific to each agent, we were inspired by [40, 43] to consider a decentralized update of each agent’s policy where we fix the rest $I - 1$ agents’ policy π_{-i} and train policy π_i to get the best response of agent i . In this paper, we updated π_i by iteratively optimizing the following objective:

$$\pi_i^j = \arg \max \mathbb{E}_{\pi_i, \mu_0} [\bar{V}_{i,t}^{\pi_i, \pi_{-i}^{j-1}, r}(s)] - \eta_1 \mathcal{B}_\psi(\pi_i, \pi_i^l) - \frac{1}{\eta_2} \mathcal{B}_\psi(\pi_i, \pi_i^{j-1}) \quad (10)$$

where π_i^l denotes the imitation policy learned by the world model (Equation 9), and the π_i^{j-1} denotes the policy learned from the previous iteration. This objective contains several key components that can efficiently facilitate convergence to a CCE by utilizing:

Optimistic V-learning. Inspired by [57], our optimistic value function is defined by:

$$\bar{V}_{i,t}^{\pi_i, \pi_{-i}}(s) = \mathbb{E}_{\mu_0, \mathcal{T}, \pi_i, \pi_{-i}} \left[\sum_{\iota=t}^T \gamma^\iota [r_i(o_\iota, a_\iota) + \beta_i(o_\iota)] \mid o_0 = \mathcal{O}(s_{t+1}) \right] \quad (11)$$

where $\beta_i(o) = \frac{c}{\rho_i(o)}$ serves as an exploration bonus to less visited state. c is a hyper-parameter, and $\rho_i(o)$ denotes the density of visited observation o [64], representing the probability of o occurrences at time t [65]. Such an optimistic V-learning objective serves as an extension to the CCE-V-Learning algorithm [38, 40], which has been proven to converge to CCE under discrete environments, and we extend this algorithm to solve continuous decision-making problems.

Magnetic Mirror Descent (MMD). We follow [43] and incorporate the Bregman divergence $\mathcal{B}_\psi(\cdot, \cdot)$ with respect to the mirror map ψ such that $\mathcal{B}_\psi(x, y) = \psi(x) - \psi(y) - \langle \nabla \psi(y), x - y \rangle$ into the objective with convergence guarantees. Recent studies [41–44] confirmed that the mirror decent approaches can solve different kinds of games in multi-player settings. To derive a more intuitive objective, we implement the mirror map as the negative entropy such that $\psi(x) = \sum p(x) \log p(x)$, and the objective (12) becomes:

$$\pi_{i,t}^j = \arg \max \mathbb{E}_{\pi_i, \mu_0} [\bar{V}_{i,t}^{\pi_i, \pi_{-i}^{j-1}, r}(s)] - \eta_1 \mathcal{D}_{kl}(\pi_i \parallel \pi_i^l) - \frac{1}{\eta_2} \mathcal{D}_{kl}(\pi_i \parallel \pi_i^{j-1}) \quad (12)$$

where \mathcal{D}_{kl} is the KL-divergence of two variables. Intuitively, by punishing the distance between current policy π_i and imitation policy π_i^m , this objective ensures the fidelity in the offline MARL problem (Definition 2). By constraining the scale of updates between current policy π_i and previous policy π_i^{j-1} , the training process becomes more stable. By default our objective considers the trajectory-generating τ_i probability:

$$\pi_i(\tau_i) = \mu_0(s_0) \prod_{t=0}^{T-1} [\mathcal{T}(s_{t+1} \mid s_t, \mathbf{a}_t) \pi_{i,t}(a_{i,t} \mid o_{i,t}) \boldsymbol{\pi}_{-i,t}(\mathbf{a}_{-i,t} \mid \mathbf{o}_{-i,t})]^{\gamma^t} \quad (13)$$

However, both the transition function \mathcal{T} and policy of other players $\boldsymbol{\pi}_{-i,t}$ are not subject to optimization in the objective (12), and thus recent studies [66, 67] have often considered the

discounted causal entropy [68] $\sum_{t=0}^T \gamma^t \mathcal{H}[\pi(a_{i,t}|o_{i,t})]$. Similarly, instead of utilizing the computationally intractable trajectory-level KL-divergence $\mathcal{D}_{kl}(\pi_i \|\pi_i^{j-1})$, we consider the time-wise causal KL-divergence $\sum_{t=0}^T \gamma^t \mathcal{D}_{kl}[\pi_{i,t}(\cdot) \|\pi_{i,t}^{j-1}(\cdot)]$, and by substituting it and the equation (11) into the objective (12), we have:

$$\max \mathbb{E} \left[\sum_{t=0}^T \gamma^t \left(r_i(o_t, a_t) + \beta_i(o_t) - \eta_1 \mathcal{D}_{kl}[\pi_{i,t}(\cdot) \|\pi_{i,t}^l(\cdot)] - \frac{1}{\eta_2} \mathcal{D}_{kl}[\pi_{i,t}(\cdot) \|\pi_{i,t}^{j-1}(\cdot)] \right) \right] \quad (14)$$

where, for brevity, we denote $\pi_{i,t}(a_{i,t}|o_{i,t})$ as $\pi_{i,t}(\cdot)$. This objective maximizes the rewards under the guarantee of fidelity and stability, which aligns well with the RL paradigm. Since $\mathcal{D}_{kl}(x, y) = \mathcal{H}(x, y) - \mathcal{H}(x)$, objective (14) can be further derived as:

$$\max \mathbb{E} \left[\sum_{t=0}^T \gamma^t \left(r_i^*(o_t, a_t) + \eta \mathcal{H}[\pi_{i,t}(\cdot)] \right) \right] \quad (15)$$

where for brevity, we denote $\eta = \frac{1+\eta_1\eta_2}{\eta_2}$ and $r_i^*(o_t, a_t) = r_i(o_t, a_t) + \beta_i(o_t) + \mathbb{E}_{\pi_{i,t}}[\log(\pi_{i,t}^o)^{\eta_1} (\pi_{i,t}^{j-1})^{\frac{1}{\eta_2}}]$. This objective maximizes the entropy of learned policy $\pi_{i,t}$, which aligns well with the RL paradigm.

Adjusting the Level of Competition Among Heterogeneous Agents

To effectively simulate complex traffic scenarios that include various vehicle types, such as cars, buses, and trucks, and diverse driving styles, such as aggressive and conservative driving, it is crucial to tailor the behavior of each agent to regulate the level of competition within the scenarios created. We can more thoroughly assess the system’s robustness by subjecting the AV control system to these various scenarios. This comprehensive evaluation helps in developing trustworthy AV vehicles capable of performing reliably in realistic traffic conditions. To accurately represent the diverse levels of scenarios characterized by different CCEs, we incorporate constrained and risk-sensitive policy optimization into the multi-agent traffic simulation system.

To accurately represent diverse levels of scenarios characterized by the CCEs, we incorporate the constrained and risk-sensitive policy optimization into the multi-agent traffic simulation system.

Constrained Traffic Simulation. To dynamically adjust the intensity of CCEs, we request the agents to impose varying levels of driving constraints on the AV agents, thereby modulating the severity and nature of the driving conditions. Specifically, we expand the objective (15) by formulating the trade-off between rewards and costs under a constrained policy optimization objective:

$$\arg \max_{\pi} \mathbb{E}_{\pi, \mathcal{T}, \mu_0} \left[\sum_{t=0}^T \gamma^t \left(r^*(o_{i,t}, a_{i,t}) + \eta \mathcal{H}[\pi_{i,t}(\cdot)] \right) \right] \text{ s.t. } \mathbb{E} \left[\sum_{t=0}^T \gamma^t c(o_{i,t}, a_{i,t}) \right] \leq \epsilon \quad (16)$$

where c represents the cost function aligning to different constraints. In this study, we mainly explore how the distance constraint influences the resulting CCE from our algorithm. Additionally, we can set different vehicle distance constraints to achieve varying intensities of CCE. As the distance between vehicles increases, the competitiveness among agents decreases.

Algorithm 1 TrafficGamer for capturing CCE

Input: Offline dataset \mathcal{D}^l , the number of total agents I , constraint threshold ϵ , Lagrange multiplier λ , rollout rounds B , update rounds K , loss parameters λ_1 and λ_2 , clipping parameter ω , value functions $\bar{V}_{\phi_{i,t}^r}^{\pi_i, \pi_{-i, j-1}}$, risk measure ρ , GAE lambda λ_g , distributional cost value critic $\{Z_i^c\}_{i=1}^I$, the policies $\{\pi_{\theta_i}\}_{i=1}^I$

Output: $\{\pi_{\theta_i}^{CCE}\}_{i=1}^I$

Initialize the world model \mathcal{M}_θ^l , observation o_0 from Dec-POCMDP and the roll-out dataset D_{roll} ;

for $n = 1, 2, \dots, N$ **do**

Retrieve the n^{th} scenario (including trajectories $\{\tau_{n,i}\}_{i=1}^I$ and map ζ_n) from \mathcal{D}^l ;

Update the world model \mathcal{M}_θ^l : $\mathcal{L} = -\mathbb{E}_{\mathcal{D}^l} \left[\underbrace{\prod_{k=0}^K \left(\sum_{t=0}^T \log \left(\omega_i^k p(a_{i,t}^l \mid \mu_{i,t}^k, b_{i,t}^k) \right)} \right)}_{\text{regression_loss}} + \underbrace{\log \left(\omega_i^k(s_T) \right)}_{\text{classification_loss}} \right]$

end for

for $n = 1, 2, \dots, N$ **do**

Retrieve the n^{th} scenario (including trajectories $\{\tau_{n,i}\}_{i=1}^I$ and map ζ_n) from \mathcal{D}^l ;

for $b = 1, 2, \dots, B$ **do**

For each agent i :

Perform roll-out with the policy π_θ in the n^{th} scenario;

Collect trajectories $\tau_{i,b} = [o_{i,0}, a_{i,0}, r_{i,0}, c_{i,0}, \dots, o_{i,T}, a_{i,T}, r_{i,T}, c_{i,T}]$;

Calculate reward advantages $A_{i,t}^r$ and total rewards $R_{i,t}$ from the trajectory;

Calculate cost advantages $A_{i,t}^c = \sum_{\iota=t}^T (\gamma \lambda_g)^\iota [c_{i,\iota} + \gamma \rho(Z^c(o_{i,\iota+1})) - \rho(Z^c(o_{i,\iota}))]$

Add samples to the dataset $D_{roll} = \mathcal{D}_{roll} \cup \{o_{i,t}, a_{i,t}, r_{i,t}, c_{i,t}, A_{i,t}^r, R_{i,t}, A_{i,t}^c\}_{t=1}^T$;

end for

for $i = 1, 2, \dots, I$ **do**

for $k = 1, 2, \dots, K$ **do**

Sample a data point $o_{i,k}, a_{i,k}, r_{i,k}, c_{i,k}, A_{i,k}^{\pi,r}, R_{i,k}, A_{i,k}^{\pi,c}$;

Calculate the clipping loss: $L^{\text{CLIP}}(\theta_{i,k}) = \min \left[\left(\frac{\pi_{\theta_{i,k}}(\cdot)}{\pi_{\theta_{old}}(\cdot)} A_{i,k}^r, \text{clip} \left(\frac{\pi_{\theta_{i,k}}(\cdot)}{\pi_{\theta_{old}}(\cdot)}, 1 - \omega, 1 + \omega \right) A_{i,k}^r \right) + \eta \mathcal{H}[\pi_{\theta_{i,k}}(\cdot)] - \lambda (A_{i,k}^c - \epsilon) \right]$

Calculate the value function loss: $L^{VF} = \|\bar{V}_{\phi_{i,k}^r}^{\pi_i, \pi_{-i, j-1}}(s_k) - R\|_2^2$

Update policy parameters by minimizing the loss: $-L^{\text{CLIP}} + \lambda_1 L^{VF} - \lambda_2 \mathcal{H}(\pi_i)$

Update the cost distribution Z_i^c by distributional Bellman operator with the equation 18

end for

Update the Lagrange multiplier by minimizing the loss: $L^\lambda: \lambda [\mathbb{E}_{D_{roll}}(\hat{A}_i^c) - \epsilon]$

end for

end for

Risk-sensitive Traffic Simulation. This strategy explicitly manages the risk sensitivity of driving behaviors, thereby deriving risk-seeking or risk-averse policies for each AV agent. This approach effectively promotes either aggressive or conservative driving policies to enhance the realism and variability of the scenarios. With the aim of guiding risk-sensitive and constraints-satisfying policies for multiple agents, inspired by [55], we develop a risk-sensitive constraint to capture the uncertainty induced by environmental dynamics and extend the Objective 16 as follows:

$$\arg \max_{\pi} \mathbb{E}_{\pi, \mathcal{T}, \mu_0} \left[\sum_{t=0}^T \gamma^t \left(r^*(o_{i,t}, a_{i,t}) + \eta \mathcal{H}[\pi_{i,t}(\cdot)] \right) \right] \text{ s.t. } \rho_{\alpha} \left[\sum_{t=0}^T \gamma^t C(\mathcal{O}_{i,t}(s_t), A_{i,t}) \right] \leq \epsilon \quad (17)$$

where C is the cost variable and α represents confidence. To specify the risk measure, we define the corresponding risk envelope $\mathcal{U}_{\alpha}^{\pi_i} = \{\zeta_{\alpha} : \Gamma \rightarrow [0, \frac{1}{\alpha}] \mid \sum_{\tau_i \in \Gamma} \zeta(\tau_i) \pi_i(\tau_i) = 1\}$, characterized as a compact, convex, and bounded set. This envelope guides the risk measure, which is induced by a distorted probability distribution for each agent $\pi_i^{\zeta}(\tau_i) = \zeta \cdot \pi_i(\tau_i)$. For example, the Conditional Value-at-Risk (CVaR) can be defined as $\rho_{\alpha}^{\pi_i}[\sum_{t=0}^T \gamma^t c_{i,t}] = \sup_{\zeta_{\alpha} \in \mathcal{U}_{\alpha}^{\pi_i}} \mathbb{E}_{\tau_i \sim p^{\pi_i}} [\zeta_{\alpha}(\tau_i) \sum_{t=0}^T \gamma^t c_{i,t}]$.

Constructing the distorted probability-based risk measure relies on the estimated distribution of discounted cumulative costs. To estimate this distribution, we define the variable of discounted cumulative costs as $Z^c(o_{i,t}) = \sum_{\iota=0}^{T-t} \gamma^{\iota} C_{\iota} \mid \mathcal{O}_0 = o_{i,t}$ [69]. During fine-tuning, the stochastic POCMDP process can be captured by the distributional Bellman equation [56, 70]:

$$Z^c(o_{i,t}) \stackrel{\Delta}{=} C(o_{i,t}, a_{i,t}) + \gamma Z^c(\mathcal{O}_{i,t+1}(s_{t+1})) \text{ where } s_{t+1} \sim \mathcal{T}(\cdot \mid s_t, a_{i,t}) \text{ and } a_{i,t} \sim \pi_{i,t}(\cdot \mid o_{i,t}) \quad (18)$$

Following [71], we parameterize the distribution with N supporting quantiles and update these function via quantile regression [56], which acts as an asymmetric squared loss in an interval $[-\kappa, \kappa]$ around zero:

$$\rho_{\tau_q}^{\kappa}(u) = |\tau_q - \delta_{\{u < 0\}}| \mathcal{L}_{\kappa}(u) \text{ where } \mathcal{L}_{\kappa}(u) = \begin{cases} \frac{1}{2}u^2, & \text{if } |u| \leq \kappa \\ \kappa(|u| - \frac{1}{2}\kappa), & \text{otherwise} \end{cases} \quad (19)$$

τ_q is the quantile, δ denotes a Dirac and $\mathcal{L}_{\kappa}(u)$ is a Huber loss. Under these formulations, the risk-sensitive advantage function $A_{i,t}^c$ can be computed with 1-step TD updates such that $A_{i,t}^c = c_{i,t} + \gamma \rho(Z^c(o_{i,t+1})) - \rho(Z^c(o_{i,t}))$. To effectively optimize (17) by updating the Lagrange multipliers, we design a multi-agent constrained policy gradient algorithm to update the policy $\pi_{i,t}(a_{i,t} \mid o_{i,t})$ under the CTDE framework [51, 72] (see Algorithm 1). Implementation details of the specific actor and critic networks can be found in Supplementary Section 1e. By utilizing the risk-sensitivity optimization with the CVaR method, we can adjust the convince α to control whether the policy exhibits risk-seeking or risk-avoidance behavior. The larger α is, the more the policy tends to accept risk-seeking behavior.

Data availability

The Argoverse 2 dataset we used to train TrafficGamer is publicly available at <https://www.argoverse.org/> for non-commercial usage. The Waymo dataset we used to train TrafficGamer is publicly available at <https://waymo.com/open/> for non-commercial usage. The background image of the simulated Argoverse 2 and Waymo environment is from the Argoverse 2 and Waymo dataset. Source data for figures are provided in this paper.

Code availability

The Scenarionet simulation platform is publicly available at <https://github.com/metadriaverse/scenarionet>. The av2-api is available at <https://github.com/argoverse/av2-api>. The waymo-api is available at <https://github.com/waymo-research/waymo-open-dataset>. The source code used to analyze experiment results is publicly available at <https://github.com/qiaoguanren/TrafficGamer>.

References

- [1] López, P. Á. *et al.* Microscopic traffic simulation using SUMO. In *International Conference on Intelligent Transportation Systems, (ITSC)* (2018).
- [2] Zhang, H. *et al.* Cityflow: A multi-agent reinforcement learning environment for large scale city traffic scenario. In *The World Wide Web Conference, (WWW)* (2019).
- [3] Shah, S., Dey, D., Lovett, C. & Kapoor, A. Airsim: High-fidelity visual and physical simulation for autonomous vehicles. In *Field and Service Robotics* (2017).
- [4] Yang, Z. *et al.* Unisim: A neural closed-loop sensor simulator. In *IEEE/CVF Conference on Computer Vision and Pattern Recognition, (CVPR)* (2023).
- [5] Leurent, E. An environment for autonomous driving decision-making (2018).
- [6] Cai, P., Lee, Y., Luo, Y. & Hsu, D. SUMMIT: A simulator for urban driving in massive mixed traffic. In *International Conference on Robotics and Automation, (ICRA)* (2020).
- [7] Li, Q. *et al.* Metadrive: Composing diverse driving scenarios for generalizable reinforcement learning. *IEEE Trans. Pattern Anal. Mach. Intell., (TPAMI)* (2023).
- [8] Wang, X., Krasowski, H. & Althoff, M. Commonroad-rl: A configurable reinforcement learning environment for motion planning of autonomous vehicles. In *IEEE International Intelligent Transportation Systems Conference, (ITSC)* (2021).
- [9] Sun, Q., Huang, X., Williams, B. C. & Zhao, H. Intersim: Interactive traffic simulation via explicit relation modeling. In *IEEE/RSJ International Conference on Intelligent Robots and Systems, (IROS)* (2022).
- [10] Xu, D., Chen, Y., Ivanovic, B. & Pavone, M. Bits: Bi-level imitation for traffic simulation. In *IEEE International Conference on Robotics and Automation, (ICRA)* (2023).
- [11] Gulino, C. *et al.* Waymax: An accelerated, data-driven simulator for large-scale autonomous driving research. *CoRR* **abs/2310.08710** (2023).
- [12] Lavington, J. W. *et al.* Torchdriveenv: A reinforcement learning benchmark for autonomous driving with reactive, realistic, and diverse non-playable characters. *arXiv preprint arXiv:2405.04491* (2024).
- [13] Gao, D. *et al.* Cardreamer: Open-source learning platform for world model based autonomous driving. *arXiv* (2024).
- [14] Simulation, M. Carsim (2024). URL <https://www.carsim.com>.
- [15] MathWorks, T. Vehicle dynamics blockset: Model and simulate vehicle dynamics in a virtual 3d environment (2024). URL <https://www.mathworks.com/products/vehicle-dynamics.html>.

- [16] Dosovitskiy, A., Ros, G., Codevilla, F., Lopez, A. & Koltun, V. CARLA: An open urban driving simulator. In *Conference on Robot Learning, (CoRL)* (2017).
- [17] Nvidia. Nvidia drive end-to-end platform for software-defined vehicles (2024). URL <https://www.nvidia.com/en-us/self-driving-cars/>.
- [18] VI-grade. Driving simulators: An invaluable set of tools to successfully accelerate your development process (2023). URL <https://www.vi-grade.com/en/solutions/driving-simulators>.
- [19] Ding, W. *et al.* A survey on safety-critical driving scenario generation - A methodological perspective. *IEEE Transactions on Intelligent Transportation Systems(TIPS)* (2023).
- [20] Bergamini, L. *et al.* Simnet: Learning reactive self-driving simulations from real-world observations. In *IEEE International Conference on Robotics and Automation, (ICRA)* (2021).
- [21] Feng, L., Li, Q., Peng, Z., Tan, S. & Zhou, B. Trafficgen: Learning to generate diverse and realistic traffic scenarios. In *IEEE International Conference on Robotics and Automation, (ICRA)* (2023).
- [22] Suo, S., Regalado, S., Casas, S. & Urtasun, R. Trafficsim: Learning to simulate realistic multi-agent behaviors. In *IEEE/CVF Conference on Computer Vision and Pattern Recognition, (CVPR)* (2021).
- [23] Huang, Z. *et al.* Versatile scene-consistent traffic scenario generation as optimization with diffusion. *CoRR* **abs/2404.02524** (2024).
- [24] Yan, X. *et al.* Learning naturalistic driving environment with statistical realism. *Nature Communications* **14**, 2037 (2023).
- [25] Yao, Z., Li, X., Lang, B. & Chuah, M. C. C. Goal-lbp: Goal-based local behavior guided trajectory prediction for autonomous driving. *IEEE Transactions on Intelligent Transportation Systems, (TIPS)* **25**, 6770–6779 (2024).
- [26] Tan, S. *et al.* Scenegen: Learning to generate realistic traffic scenes. In *IEEE Conference on Computer Vision and Pattern Recognition, (CVPR)* (2021).
- [27] Zheng, Z., Ying, X., Yao, Z. & Chuah, M. C. C. Robustness of trajectory prediction models under map-based attacks. In *IEEE/CVF Winter Conference on Applications of Computer Vision, (WACV)* (2023).
- [28] Wang, J. *et al.* Advsim: Generating safety-critical scenarios for self-driving vehicles. In *IEEE Conference on Computer Vision and Pattern Recognition, (CVPR)* (2021).
- [29] Rempe, D., Philion, J., Guibas, L. J., Fidler, S. & Litany, O. Generating useful accident-prone driving scenarios via a learned traffic prior. In *IEEE/CVF Conference on Computer Vision and Pattern Recognition, (CVPR)* (2022).

- [30] Feng, S., Yan, X., Sun, H., Feng, Y. & Liu, H. X. Intelligent driving intelligence test for autonomous vehicles with naturalistic and adversarial environment. *Nature Communications* (2021).
- [31] Hanselmann, N., Renz, K., Chitta, K., Bhattacharyya, A. & Geiger, A. KING: generating safety-critical driving scenarios for robust imitation via kinematics gradients. In *European Conference on Computer Vision, (ECCV)* (2022).
- [32] Suo, S. *et al.* Mixsim: A hierarchical framework for mixed reality traffic simulation. In *IEEE/CVF Conference on Computer Vision and Pattern Recognition, (CVPR)* (2023).
- [33] Cao, Y. *et al.* Robust trajectory prediction against adversarial attacks. In *Conference on Robot Learning, (CoRL)* (2022).
- [34] Zhang, J., Xu, C. & Li, B. Chatscene: Knowledge-enabled safety-critical scenario generation for autonomous vehicles. In *IEEE/CVF Conference on Computer Vision and Pattern Recognition, (CVPR)* (2024).
- [35] Wang, Z., Li, X., Wei, D., Wang, L. & Huang, Y. Efficient generation of safety-critical scenarios combining dynamic and static scenario parameters. *IEEE Transactions on Intelligent Vehicles, (TIV)* (2024).
- [36] Zhang, C. *et al.* Learning realistic traffic agents in closed-loop. In *Conference on Robot Learning, (CoRL)* (2023).
- [37] Ding, W., Lin, H., Li, B. & Zhao, D. Generalizing goal-conditioned reinforcement learning with variational causal reasoning. In *Advances in Neural Information Processing Systems, (NeurIPS)* (2022).
- [38] Bai, Y., Jin, C. & Yu, T. Near-optimal reinforcement learning with self-play. In *Advances in Neural Information Processing Systems, (NeurIPS)* (2020).
- [39] Bai, Y., Jin, C., Wang, H. & Xiong, C. Sample-efficient learning of stackelberg equilibria in general-sum games. In *Advances in Neural Information Processing Systems, (NeurIPS)* (2021).
- [40] Song, Z., Mei, S. & Bai, Y. When can we learn general-sum markov games with a large number of players sample-efficiently? In *International Conference on Learning Representations, (ICLR)* (2022).
- [41] Liu, M., Ozdaglar, A. E., Yu, T. & Zhang, K. The power of regularization in solving extensive-form games. In *International Conference on Learning Representations, (ICLR)* (2023).
- [42] Cen, S., Chi, Y., Du, S. S. & Xiao, L. Faster last-iterate convergence of policy optimization in zero-sum markov games. In *International Conference on Learning Representations, (ICLR)* (2023).

- [43] Sokota, S. *et al.* A unified approach to reinforcement learning, quantal response equilibria, and two-player zero-sum games. In *International Conference on Learning Representations, (ICLR)* (2023).
- [44] Li, P. *et al.* Configurable mirror descent: Towards a unification of decision making. In *International Conference on Machine Learning, (ICML)* (2024).
- [45] Wilson, B. *et al.* Argoverse 2: Next generation datasets for self-driving perception and forecasting. In *Advances in Neural Information Processing Systems Track on Datasets and Benchmarks 1, (NeurIPS)* (2021).
- [46] Ettinger, S. *et al.* Large scale interactive motion forecasting for autonomous driving : The waymo open motion dataset. In *IEEE/CVF International Conference on Computer Vision, (ICCV)* (2021).
- [47] Zhang, Y., Zhang, R., Gu, Y. & Li, N. Multi-agent reinforcement learning with reward delays. In *Learning for Dynamics and Control Conference, (L4DC)* (2023).
- [48] Guanren, Q., Guorui, Q., Rongxiao, Q. & Guiliang, L. Modelling competitive behaviors in autonomous driving under generative world model. In *European Conference on Computer Vision, (ECCV)* (2025).
- [49] Nash, J. Non-cooperative games. *Annals of mathematics* 286–295 (1951).
- [50] Zhou, Z., Wang, J., Li, Y. & Huang, Y. Query-centric trajectory prediction. In *International Conference on Computer Vision and Pattern Recognition, (CVPR)* (2023).
- [51] Yu, C. *et al.* The surprising effectiveness of PPO in cooperative multi-agent games. In *Advances in Neural Information Processing Systems, (NeurIPS)* (2022).
- [52] Huang, Z., Liu, H. & Lv, C. Gameformer: Game-theoretic modeling and learning of transformer-based interactive prediction and planning for autonomous driving. In *International Conference on Computer Vision, (ICCV)* (2023).
- [53] Rubner, Y., Tomasi, C. & Guibas, L. The earth mover’s distance as a metric for image retrieval. *International Journal of Computer Vision, (IJCV)* **40**, 99–121 (2000).
- [54] Li, Q. *et al.* Scenarionet: Open-source platform for large-scale traffic scenario simulation and modeling. In *Advances in Neural Information Processing Systems, (NeurIPS)* (2023).
- [55] Xu, S. & Liu, G. Uncertainty-aware constraint inference in inverse constrained reinforcement learning. In *International Conference on Learning Representations, (ICLR)* (2024).
- [56] Dabney, W., Rowland, M., Bellemare, M. G. & Munos, R. Distributional reinforcement learning with quantile regression. In *AAAI Conference on Artificial Intelligence, (AAAI)* (2017).
- [57] Mao, W. & Basar, T. Provably efficient reinforcement learning in decentralized general-sum markov games. *Dynamic Games And Applications* **13**, 165–186 (2023).

- [58] Hwang, K.-S., Chiou, J.-Y. & Chen, T.-Y. Cooperative reinforcement learning based on zero-sum games. *SICE Annual Conference* 2973–2976 (2008).
- [59] Yang, Y. & Wang, J. An overview of multi-agent reinforcement learning from game theoretical perspective. *CoRR* **abs/2011.00583** (2020).
- [60] Hu, J. & Wellman, M. P. Nash q-learning for general-sum stochastic games. *Journal of Machine Learning Research, (JMLR)* **4**, 1039–1069 (2003).
- [61] Hambly, B. M., Xu, R. & Yang, H. Policy gradient methods find the nash equilibrium in n-player general-sum linear-quadratic games. *Journal of Machine Learning Research, (JMLR)* **24**, 139:1–139:56 (2023).
- [62] Brown, T. B. *et al.* Language models are few-shot learners. In *Advances in Neural Information Processing Systems, (NeurIPS)* (2020).
- [63] Zhou, Z., Wen, Z., Wang, J., Li, Y.-H. & Huang, Y.-K. Qcnex: A next-generation framework for joint multi-agent trajectory prediction. *arXiv preprint arXiv:2306.10508* (2023).
- [64] Qiao, G., Liu, G., Poupart, P. & Xu, Z. Multi-modal inverse constrained reinforcement learning from a mixture of demonstrations. In *Advances in Neural Information Processing Systems, (NeurIPS)* (2023).
- [65] Sun, Y. & Yang, S. Manifold-constrained gaussian process inference for time-varying parameters in dynamic systems. *Statistics and Computing* **33**, 142 (2023).
- [66] Haarnoja, T., Tang, H., Abbeel, P. & Levine, S. Reinforcement learning with deep energy-based policies. In *International Conference on Machine Learning, (ICML)* (2017).
- [67] Haarnoja, T., Zhou, A., Abbeel, P. & Levine, S. Soft actor-critic: Off-policy maximum entropy deep reinforcement learning with a stochastic actor. In *International Conference on Machine Learning, (ICML)* (2018).
- [68] Ziebart, B. D., Bagnell, J. A. & Dey, A. K. Modeling interaction via the principle of maximum causal entropy. In *International Conference on Machine Learning, (ICML)*, 1255–1262 (2010).
- [69] Luo, Y., Liu, G., Duan, H., Schulte, O. & Poupart, P. Distributional reinforcement learning with monotonic splines. In *International Conference on Learning Representations, (ICLR)* (2022).
- [70] Gerstenberg, J., Neining, R. & Spiegel, D. On solutions of the distributional bellman equation. *CoRR* **abs/2202.00081** (2022).
- [71] Dabney, W., Rowland, M., Bellemare, M. G. & Munos, R. Distributional reinforcement learning with quantile regression. In *AAAI Conference on Artificial Intelligence, (AAAI)*, 2892–2901 (2018).
- [72] Schulman, J., Wolski, F., Dhariwal, P., Radford, A. & Klimov, O. Proximal policy optimization algorithms. *CoRR* **abs/1707.06347** (2017).

Acknowledgment

Author contributions

G.Q.¹ and G.L. conceived and led the research project. G.Q.¹, G.Q.², and G.L. developed the framework and algorithm. G.Q.¹ and G.L. wrote the paper. G.Q.¹ and G.L. developed the experimental metrics for the algorithm. G.Q.¹ and G.Q.² implemented the algorithms and world model. G.Q.¹ and J.Y. pre-trained the world model. G.Q.¹ prepared the exploitability experiment results and fidelity experiment results. G.Q.¹, G.Q.², and J.Y. implemented the baselines. G.Q.¹ and J.Y. prepared the scenario visualization experiment results. All authors provided feedback during the manuscript revision and discussion of results. G.L. approved the submission and accepted responsibility for the overall integrity of the paper.

Competing Interests

The authors declare no competing interests.

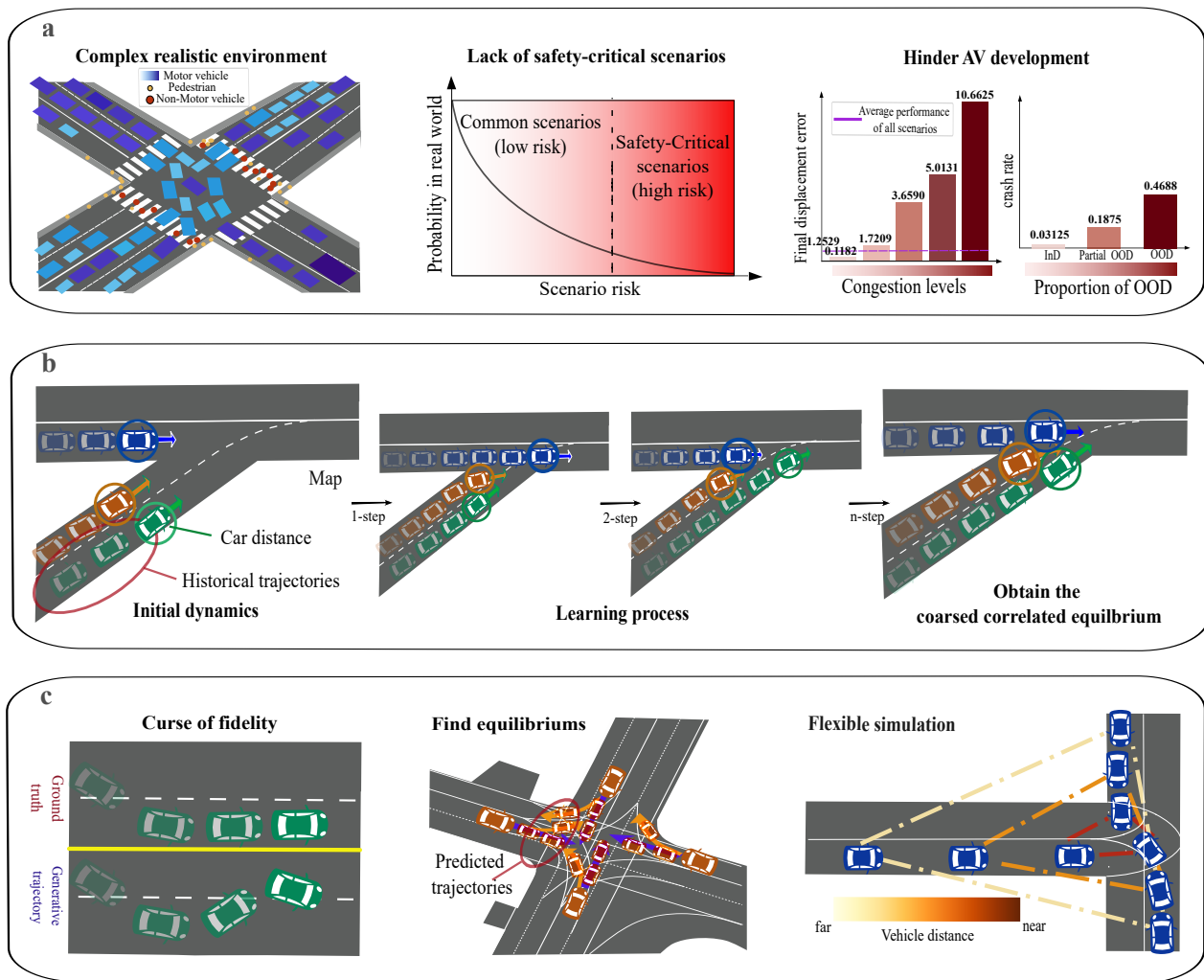


Figure 1: **Crafting flexible and reliable competitive driving scenarios with game-theoretic oracles.** **a** Complex autonomous competitive driving environments exist in reality, but the probability of these scenarios occurring is low. We lack data on such safety-critical instances to train a robust AV system. We find that, with an increase in congestion level and Out-of-Distribution (OOD) data, the performance of the AV system decreases. This greatly hinders the development of AV systems. **b** Autonomous driving scenarios encompass valuable information such as historical trajectories, map features, and interactive characteristics of surrounding vehicles. TrafficGamer can effectively capture the dynamics of competitive environments to predict future trajectories and efficiently assist each vehicle in learning optimal policies for each vehicle and solving Coarse Correlated Equilibriums (CCEs) to generate safety-critical scenarios. **c** Major challenges for generating safety-critical scenarios. The challenges include the "curse of fidelity" for future trajectory prediction, the "Finding Equilibrium" for solving the CCE during the algorithm update process, and the "controlled equilibrium" for how to control the intensity of the CCE.

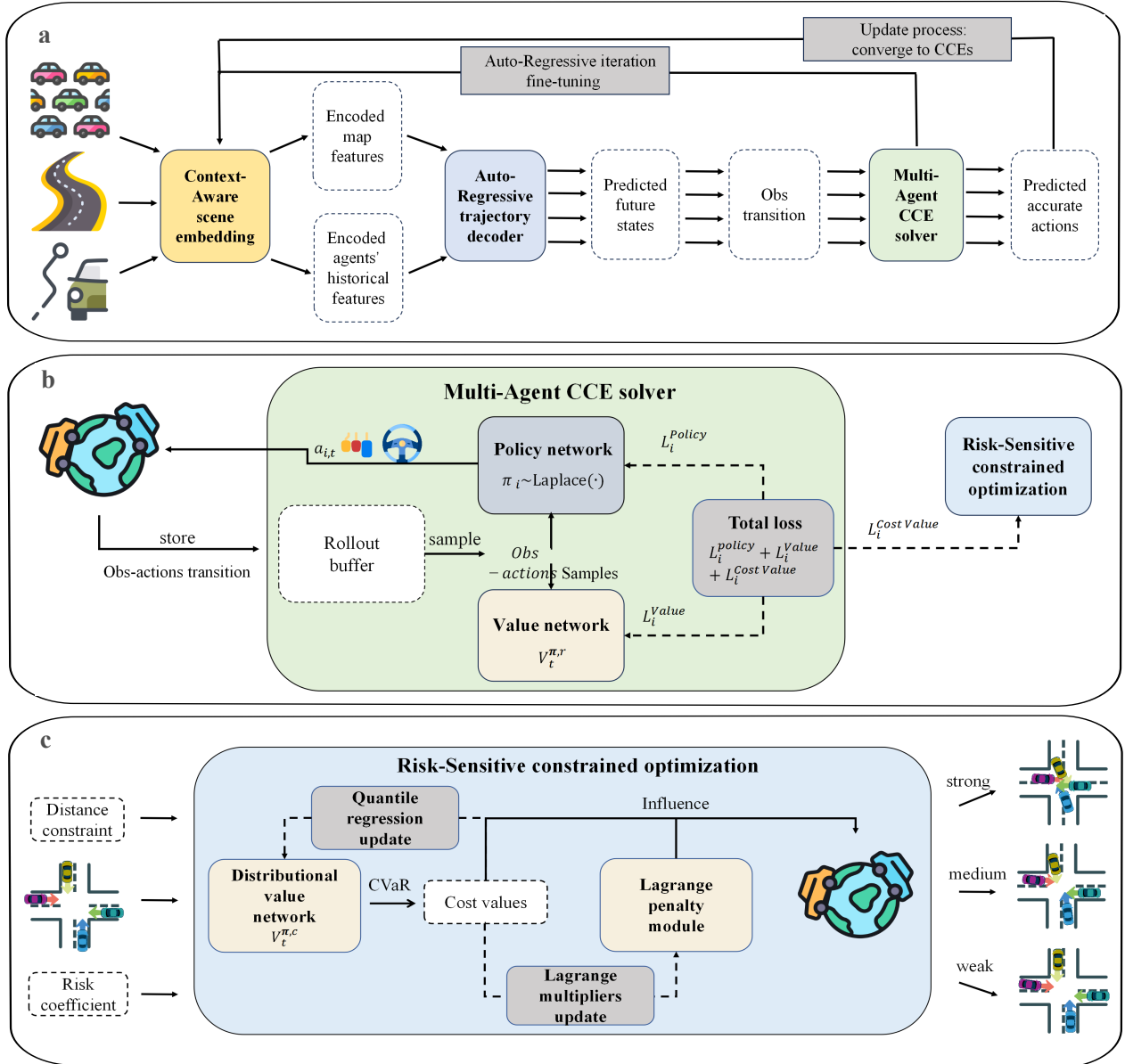


Figure 2: **Structure of TrafficGamer.** The definition of the symbols in the figure can be found in the Problem Formulation section of the Method. **a** The TrafficGamer framework consists of two parts: pre-training and fine-tuning. Initially, we utilize the training dataset to train a generative world model. Subsequently, MARL algorithms are employed to fine-tune this world model. **b** We treat the world model as the environment providing observations (Obs), with throttle and brake actions for vehicles, and design reward and cost functions to establish a Decentralized Partially Observable Markov Decision Process. Our Multi-agent CCE-Solver, combined with *optimistic V-learning update* and *magnet mirror descent*, is utilized to learn optimal policies for each agent. This process controls and captures the CCE during the learning phase. **c** We adjust *distance constraint* and *risk coefficient* to control the intensity of the CCE, thereby influencing the competitiveness of vehicles in various scenarios. By extension, we combine a *Lagrangian-based optimization* algorithm, which adopts constraints on different vehicle distances to control the CCE, and a *risk-sensitive* algorithm, which employs CVaR with different confidence levels, to affect the vehicles' risk sensitivity. The definition of the symbols in the figure can be found in the Problem Formulation section of the Methods.

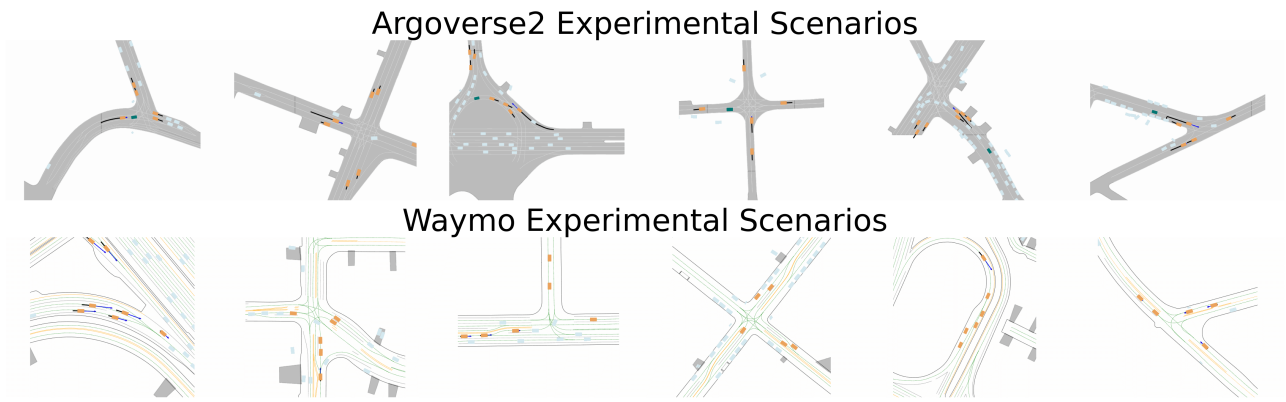


Figure 3: **Visualization of the road map.** The experimental scenarios were selected from Argoverse 2 and Waymo. The yellow cars are controlled by algorithms, green and gray cars represent environmental vehicles, black lines depict vehicle trajectories, and blue arrows indicate travel direction.

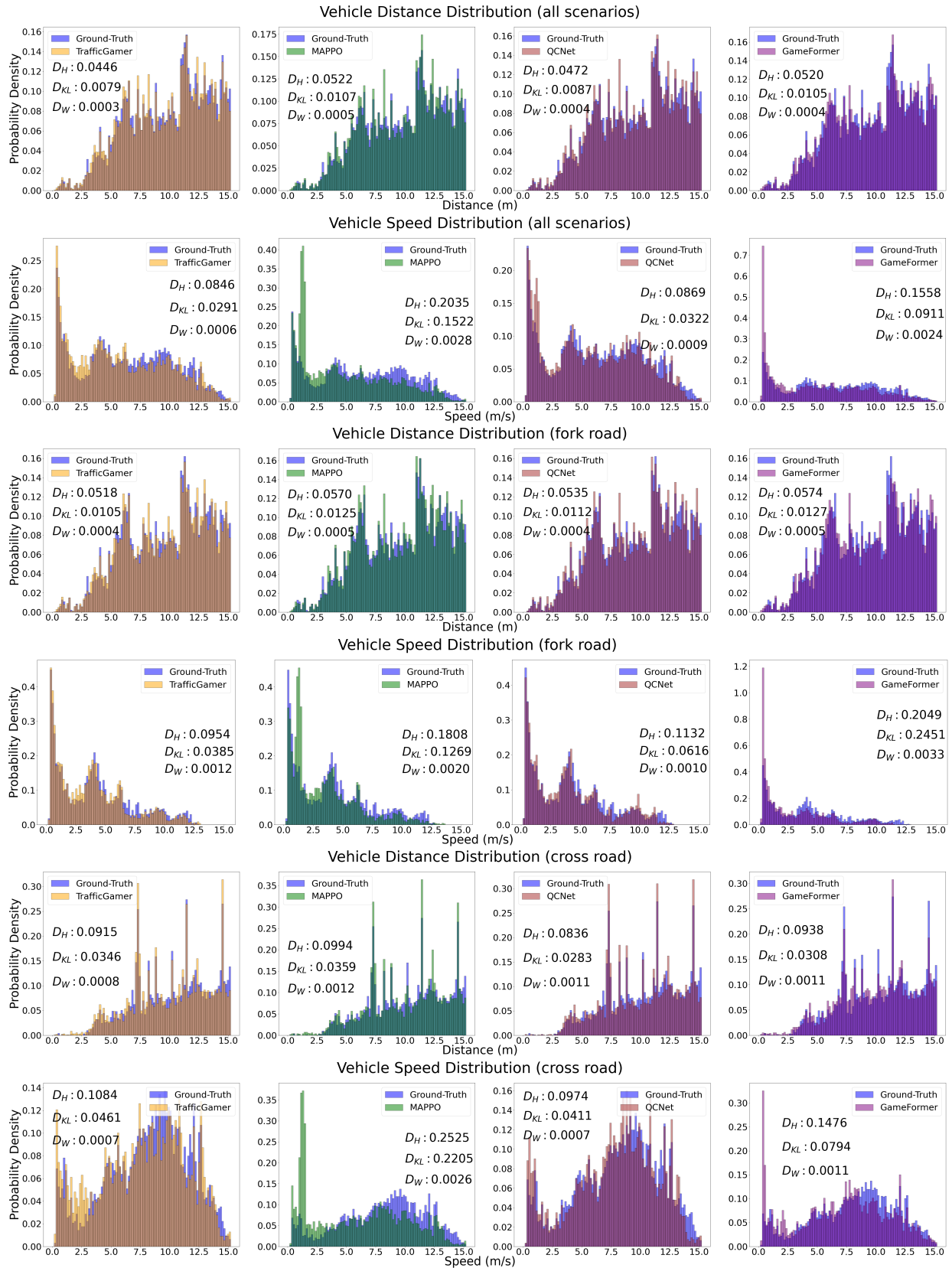


Figure 4: **Statistical realism of driving behavior.** From top to bottom are all methods' vehicle distance and speed distributions. We use various distance metrics to measure the distance between the generated and the real data distribution in three settings: all scenarios, fork road, and cross road.

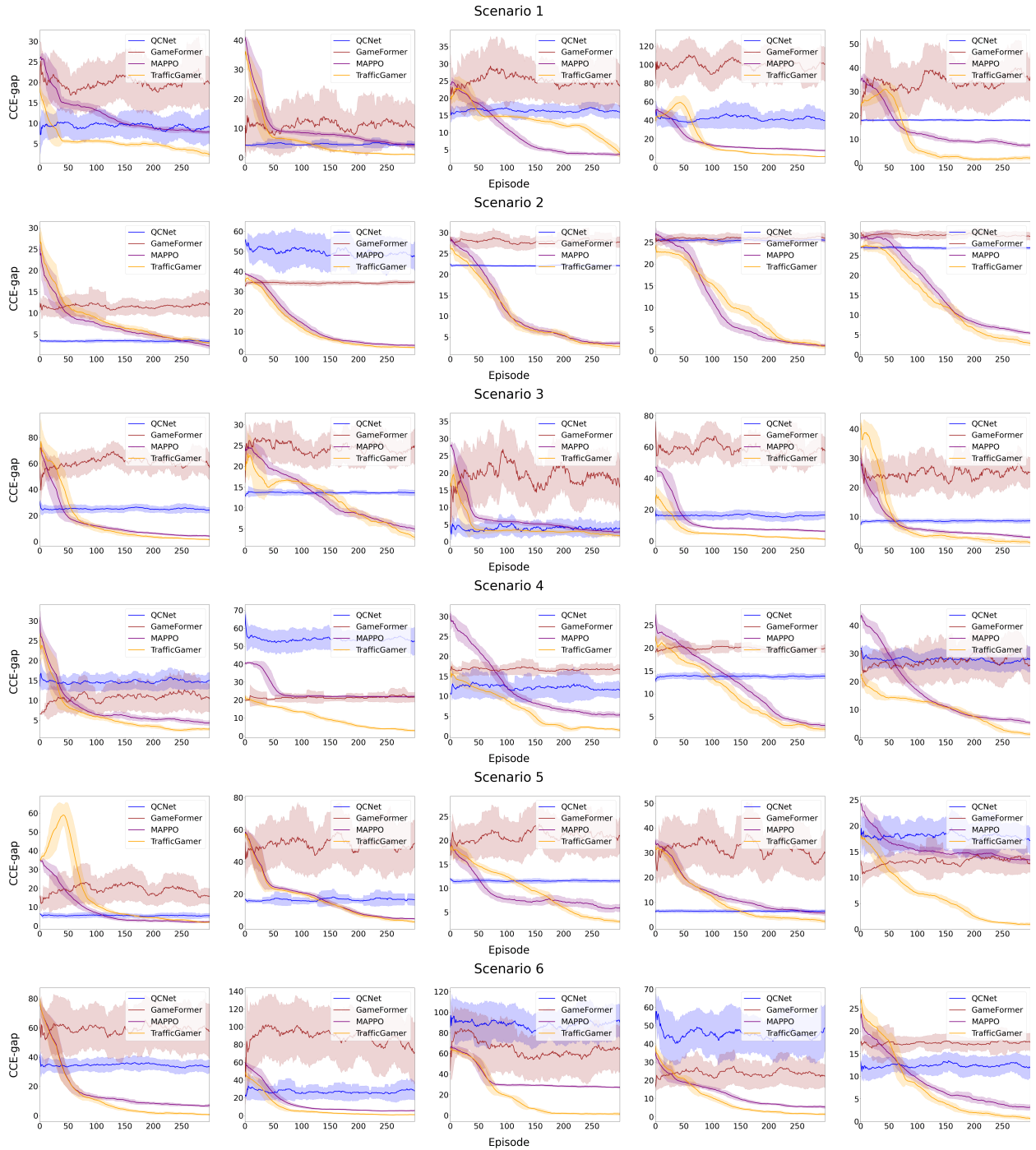


Figure 5: **CCE-gap** obtained from the **Breaking the Equilibrium** approach. Each row represents a scenario and scenarios 1-6 correspond to *Y-Junction*, *Dense-lane intersection*, *Roundabout*, *Dual-lane intersection*, *T-Junction*, and *Merge* respectively. Each column corresponds to one of the agents in the multi-agent environment. Because of the space limitations, the CCE-gap results of other agents can be seen in Supplementary Section 3a.

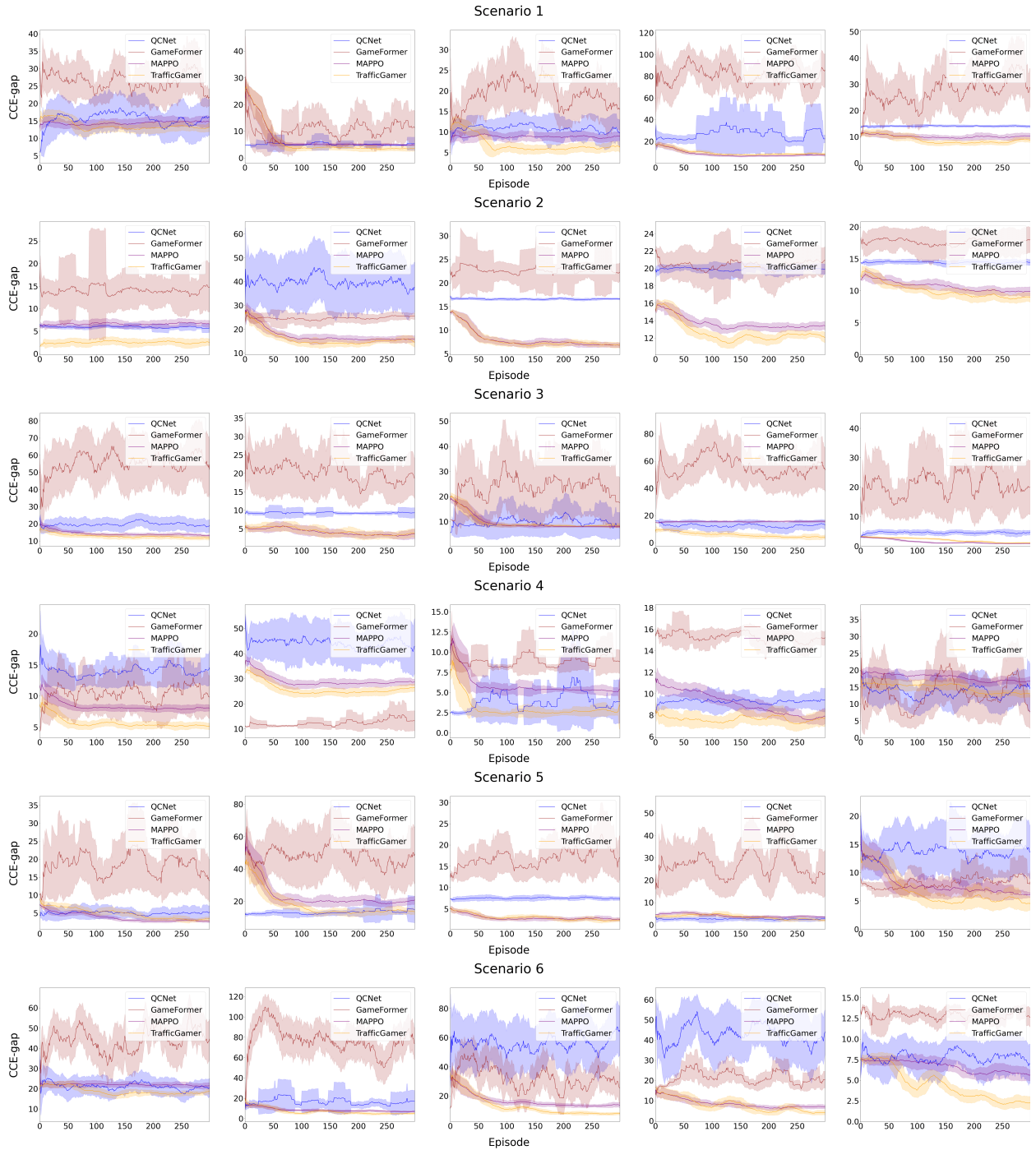
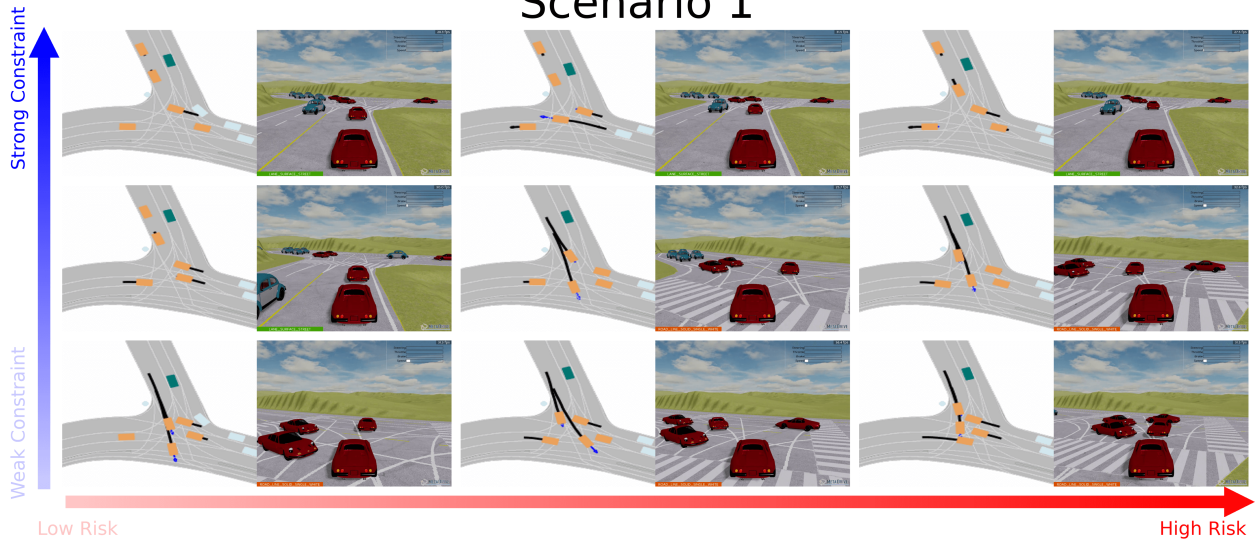
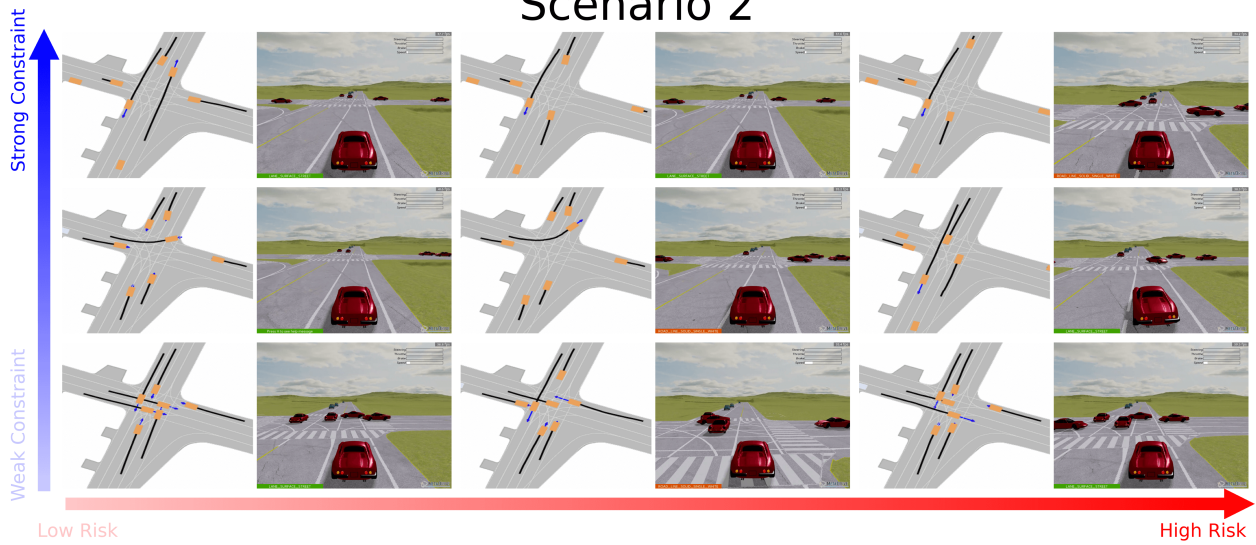


Figure 6: CCE-gap obtained from the Restricting Action Space approach. Each row represents a scenario and scenarios 1-6 correspond to *Y-Junction*, *Dense-lane intersection*, *Roundabout*, *Dual-lane intersection*, *T-Junction*, and *Merge* respectively. Each column corresponds to one of the agents in the multi-agent environment. Because of the space limitations, the CCE-gap results of other agents can be seen in Supplementary Section 3a.

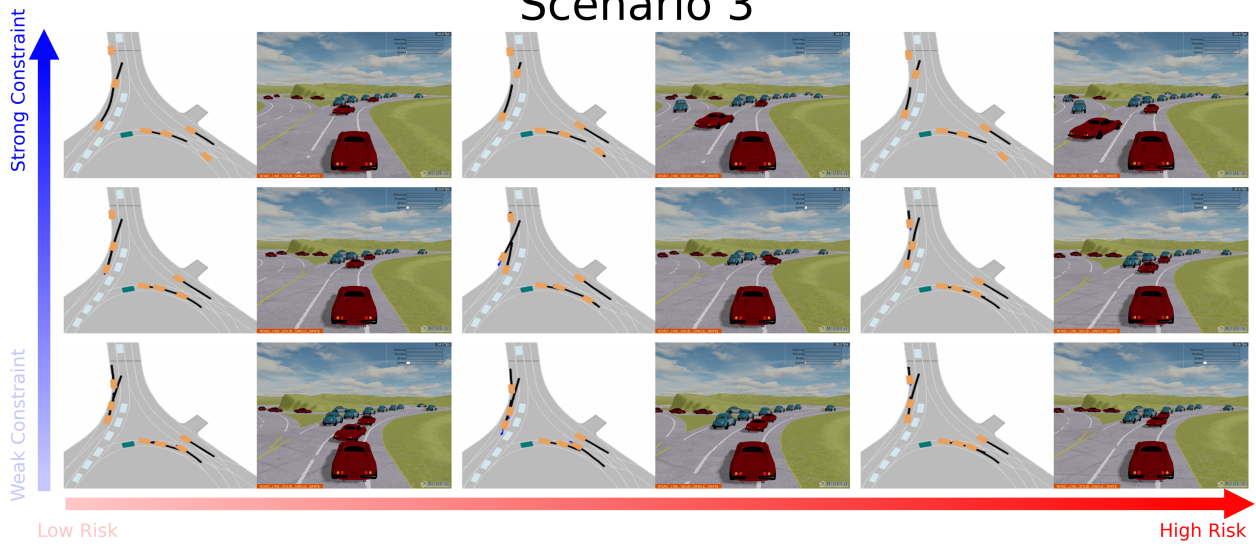
Scenario 1



Scenario 2



Scenario 3



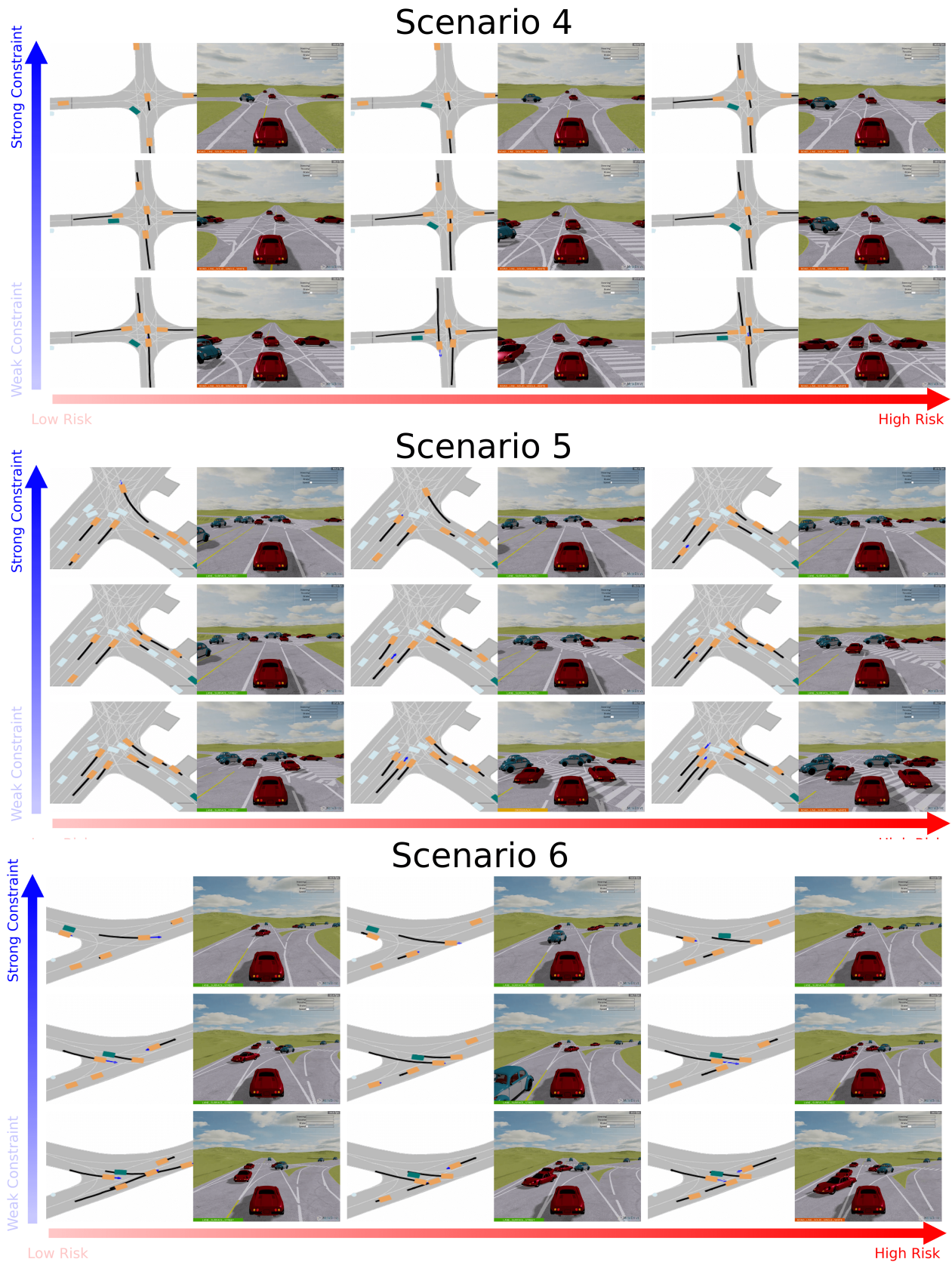
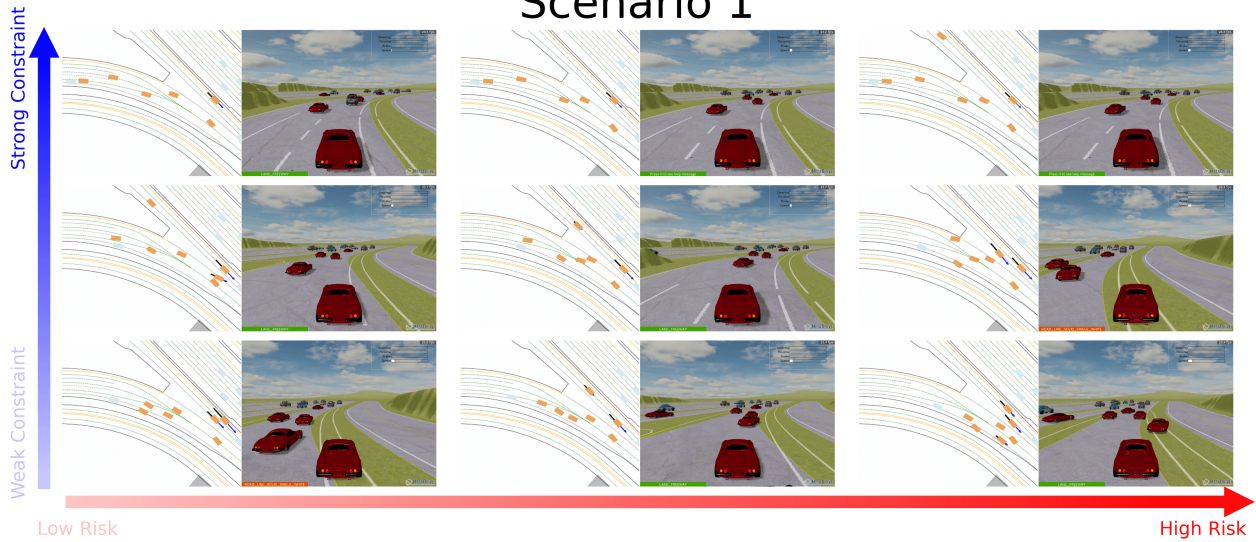
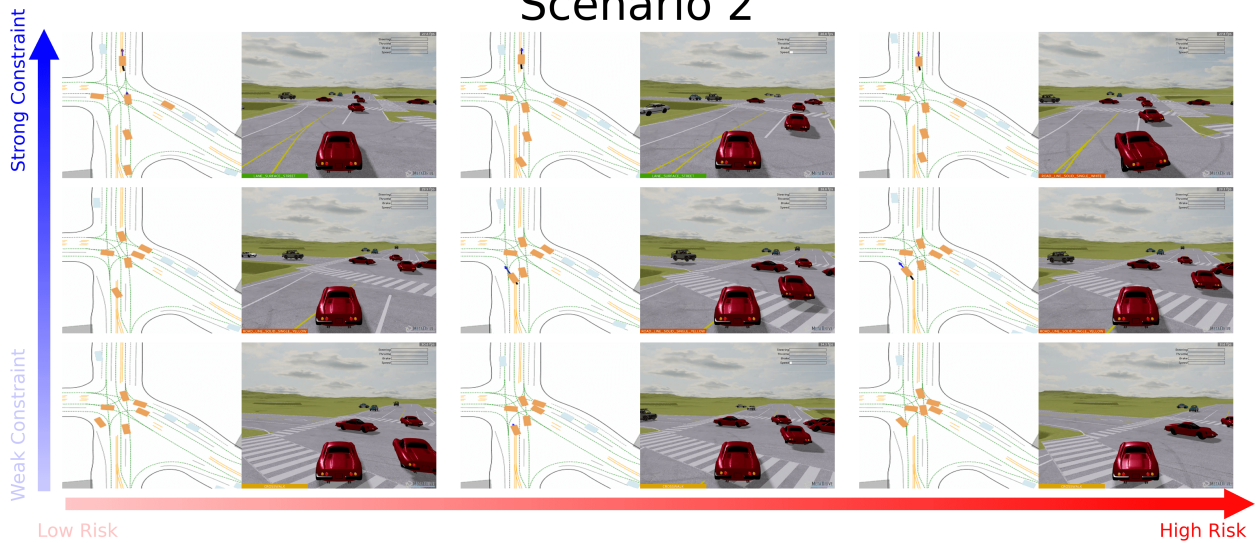


Figure 7: **Visualization of generated trajectories with high diversity (Argoverse2).** Visualization of all Argoverse2 scenarios in a 3x3 grid layout with 2D and 3D simulations. In each grid, the distance constraint relaxes from top to bottom, and the risk level strengthens from left to right. In the 2D scenes, yellow cars are algorithm-controlled, green cars and gray cars are environmental vehicles, black lines are vehicle trajectories, and blue arrows indicate travel direction. In the 3D scenes, red cars are algorithm-controlled, while blue cars represent environmental vehicles.

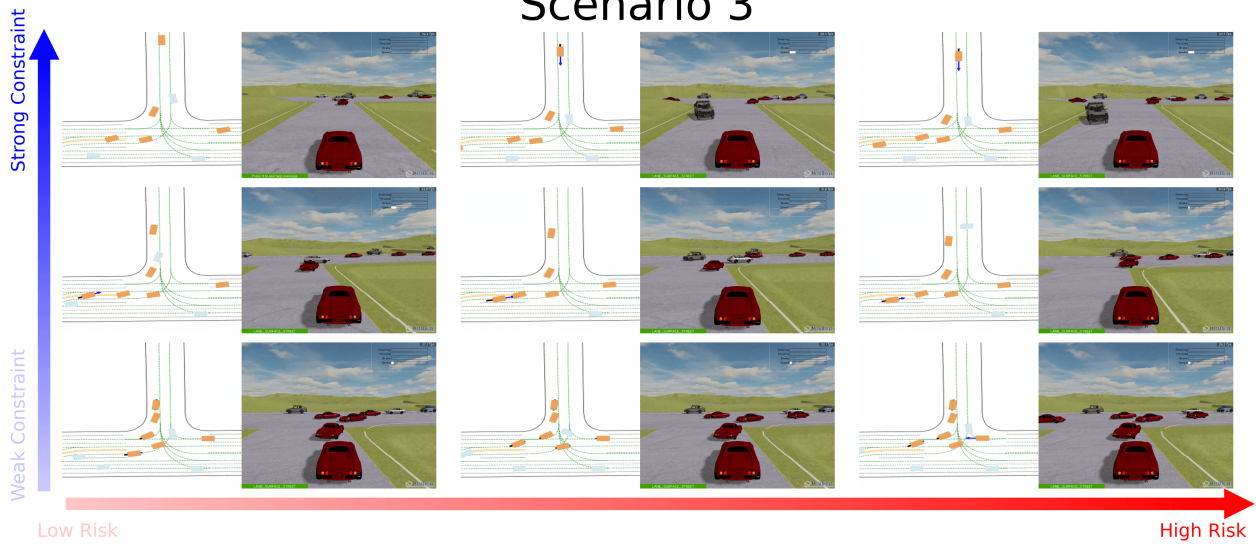
Scenario 1



Scenario 2



Scenario 3



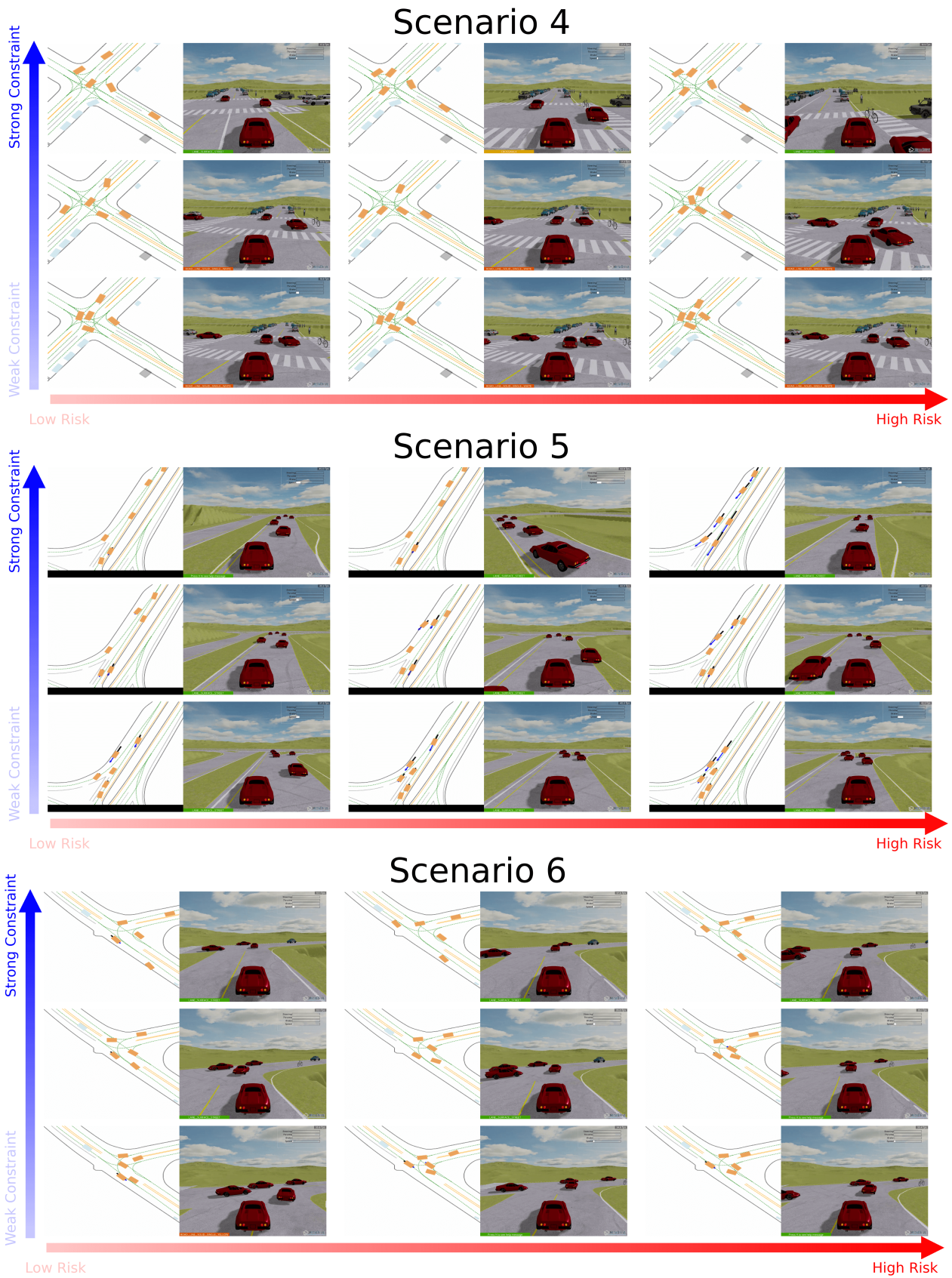


Figure 8: **Visualization of generated trajectories with high diversity (Waymo).** Visualization of all Waymo scenarios in a 3x3 grid layout with 2D and 3D simulations. In each grid, the distance constraint relaxes from top to bottom, and the risk level strengthens from left to right. In the 2D scenes, yellow cars are algorithm-controlled, green cars and gray cars are environmental vehicles, black lines are vehicle trajectories, and blue arrows indicate travel direction. In the 3D scenes, red cars are algorithm-controlled, while other cars represent environmental vehicles.

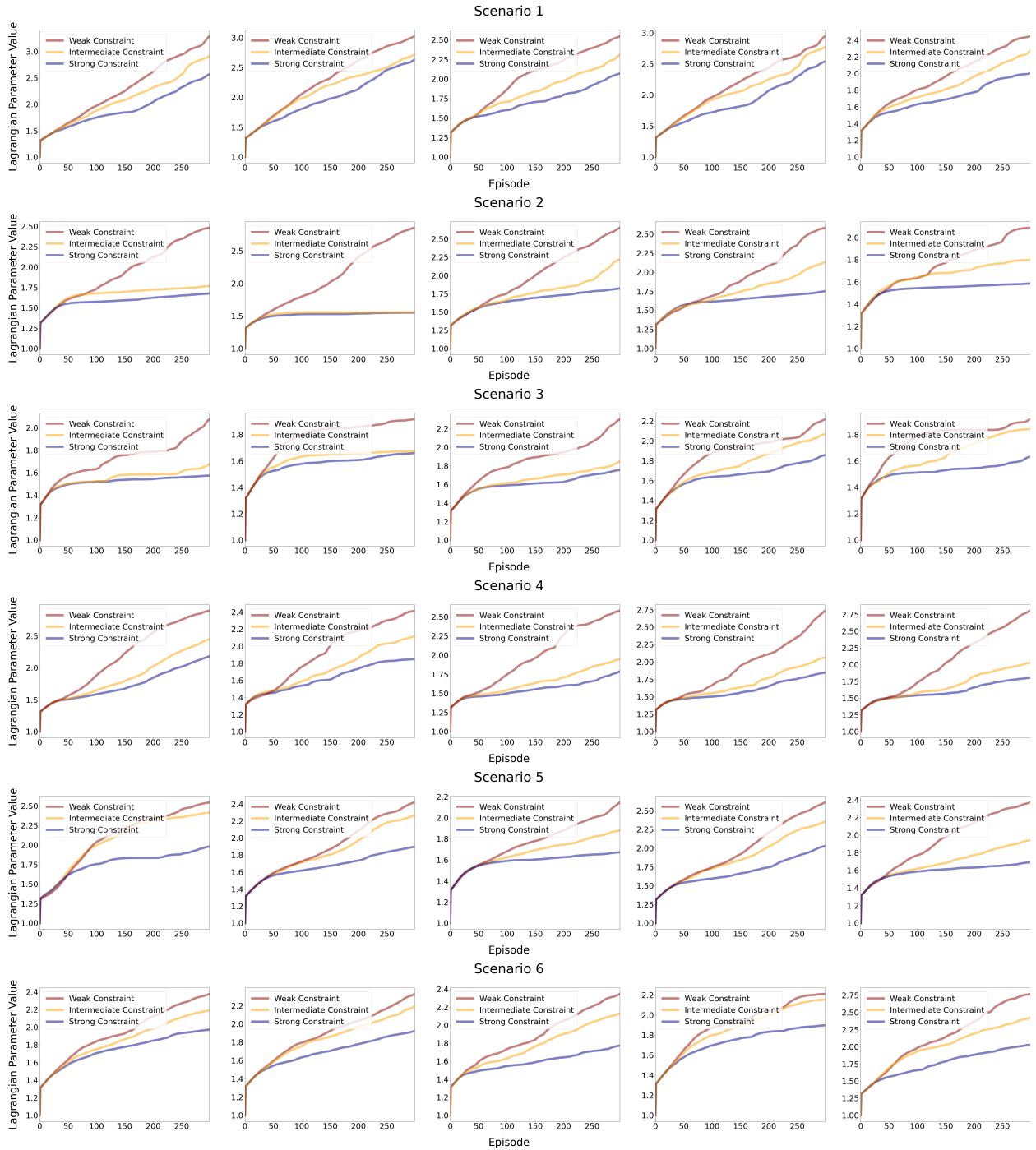


Figure 9: **Variation in Lagrangian parameters under varying constraints.** Each row represents a scenario and scenarios 1-6 correspond to *Y-Junction*, *Dense-lane intersection*, *Roundabout*, *Dual-lane intersection*, *T-Junction*, and *Merge* respectively. Each column corresponds to one of the agents in the multi-agent environment. Because of the space limitations, the Lagrangian parameter results of other agents can be seen in Supplementary Section 3b.

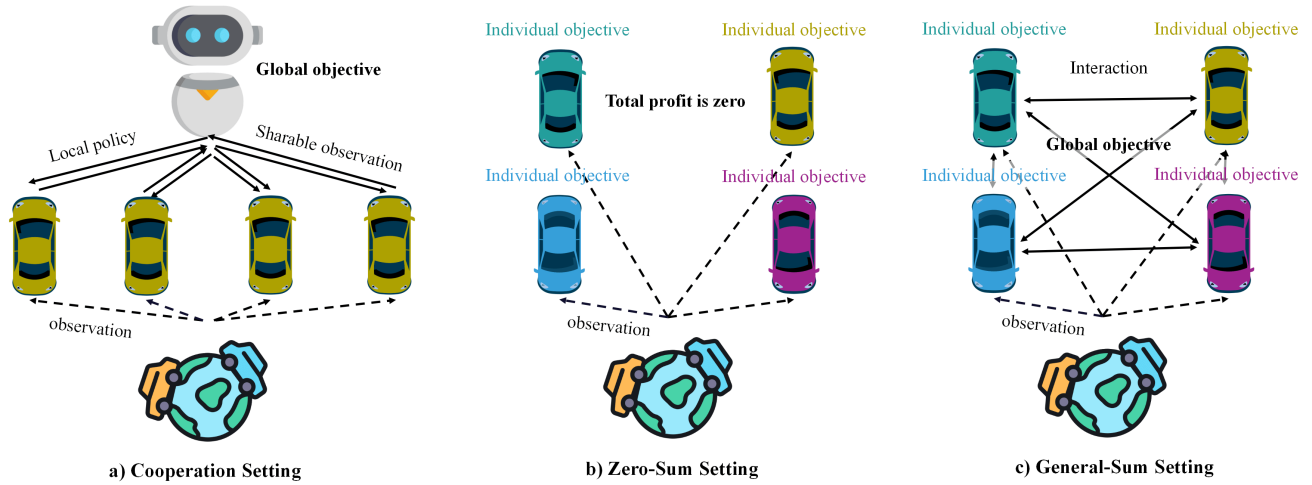


Figure 10: **Presentation of the game type.** In *cooperative games*, agents share a common interest and work together to optimize their ability to a global objective, demonstrating fully collaborative behavior. In contrast, *zero-sum games* are defined by strict competition, where one player’s gain is exactly equal to another’s loss, ensuring that the total rewards among all participants remain constant—typically zero. *General-sum games*, however, present a more complex scenario where the sum of all agents’ rewards can vary significantly. While agents may initially act competitively in these games due to self-interest, they can also maximize their benefits by collaborating with others, blending competitive and cooperative dynamics.

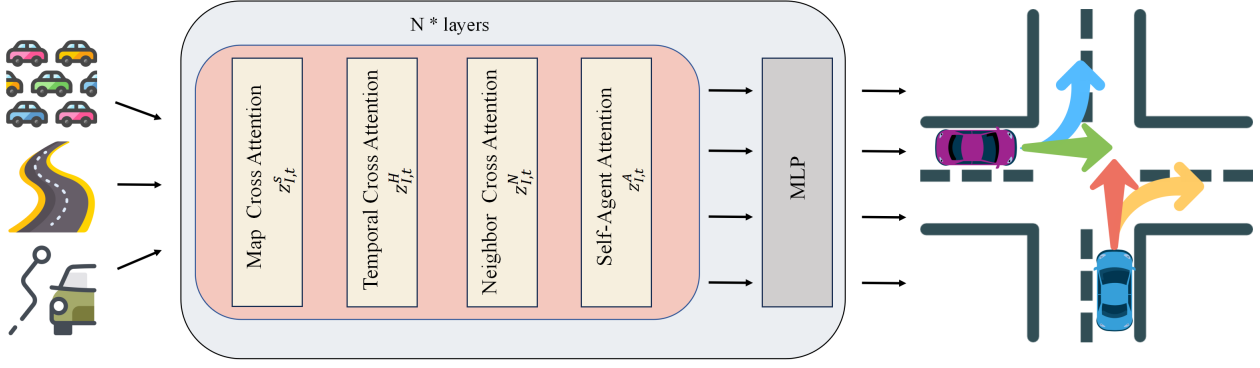


Figure 11: **Illustration of the decoder network module.** We have N attention layers to decode accurate trajectories. (1) *Agent-to-Map Cross Attention* incorporates the map information $z^m = \xi(\mathcal{M})$ (ξ is a map encoder) including all kinds of lane markings and types of polygons into the most recent agents' features such that e.g., $z_{i,t}^s = \text{CrossAttn}(\tau_{1,t}, \dots, \tau_{I,t}, z^m)$. (2) *Agent-to-Temporal Cross Attention* that embeds the historical information into the agents' trajectories $\tau_{1,t+1}, \dots, \tau_{I,t+1}$ where $\tau_{1,t+1}$ consists of $a_{1,t}$ and $s_{1,t}$, e.g., $z_{i,t}^W = \text{CrossAttn}(\{z_{i,t-1}^s, \dots, z_{i,t-W}^s\}, z_{i,t}^s)$, where H indicates the length of encoding historical steps. (3) *Agent-to-Neighbor Cross Attention* that embeds the spatial-temporal features of the surrounding agents such that $z_{i,t}^N = \text{CrossAttn}(z_{i,t}^W, \{z_{j,t}^W\}_{j \in N_i})$ and (4) *Self-Agent Attention* considers the agent's entire predicted trajectory at each time step, capturing dependencies between distant elements, e.g., $z_{i,t}^A = \text{SelfAttn}(\{z_{i,t}^N\}_{t=0}^T)$. The final state s_{t+1} is represented by concatenating $s_t = \{z_{i,w}^A\}_{w=t-W, i=0}^{t,I}$ with the predicted $z_{1,t+1}^A, \dots, z_{I,t+1}^A$.

Table 1: CCE-gap value at the last time step calculated using the Breaking the Equilibrium method

Method	Agent 1	Agent 2	Agent 3	Agent 4	Agent 5	Agent 6	Agent 7
Scenario 1							
QCNet	8.98±4.18	4.51±0.99	13.98±1.95	39.58±9.26	17.90±0.45	N/A	N/A
GameFormer	19.63±6.26	9.93±7.54	21.73±6.14	100.78±18.41	36.17±10.70	N/A	N/A
MAPPO	7.85±0.47	4.20±0.71	1.64±0.42	7.45±0.76	7.54±0.80	N/A	N/A
TrafficGamer	2.32±0.60	1.05±0.23	2.09±1.22	0.99±0.41	2.13±0.79	N/A	N/A
Scenario 2							
QCNet	3.36±0.50	47.48±7.13	22.10±0.16	25.51±0.31	26.94±0.32	35.58±4.74	6.33±2.81
GameFormer	11.81±2.59	34.69±0.78	27.75±1.29	25.95±0.95	29.90±0.99	57.80±18.25	4.04±1.62
MAPPO	2.22±0.58	3.12±0.49	3.50±0.45	1.33±0.32	5.43±0.33	4.34±0.44	3.24±0.69
TrafficGamer	2.99±0.25	2.02±0.48	2.76±0.52	1.13±0.52	2.83±0.68	2.87±0.51	1.42±1.26
Scenario 3							
QCNet	24.21±2.27	13.61±0.69	3.72±2.26	16.47±2.52	8.65±0.72	3.10±0.39	9.77±0.76
GameFormer	56.98±9.77	24.98±4.20	15.82±7.25	57.54±8.56	25.16±5.18	23.03±8.74	27.16±5.97
MAPPO	4.28±0.58	4.90±0.80	2.85±0.55	6.27±0.50	3.01±0.47	0.59±0.41	3.22±0.78
TrafficGamer	1.66±0.46	2.98±0.74	1.71±0.44	1.06±0.44	1.19±0.64	2.38±0.75	2.44±0.45
Scenario 4							
QCNet	15.08±2.04	52.62±7.41	11.54±1.89	13.83±0.56	27.96±4.47	N/A	N/A
GameFormer	10.39±3.44	21.58±2.71	16.74±1.21	19.92±0.88	25.81±6.66	N/A	N/A
MAPPO	4.36±0.58	22.02±0.67	5.33±0.65	3.05±0.49	5.38±0.59	N/A	N/A
TrafficGamer	2.78±0.34	2.98±0.55	1.48±0.37	2.22±0.50	1.21±0.61	N/A	N/A
Scenario 5							
QCNet	5.59±1.35	16.46±3.66	11.50±0.38	6.43±0.66	17.16±2.57	20.58±0.48	13.53±0.30
GameFormer	15.88±4.28	51.62±14.47	20.96±3.78	29.89±9.07	12.76±1.73	25.27±0.79	14.93±1.11
MAPPO	2.21±0.60	4.60±0.50	5.85±0.78	5.69±1.01	13.37±0.91	4.46±1.08	6.01±1.14
TrafficGamer	2.10±0.40	2.71±0.79	3.03±0.31	2.27±0.69	0.97±0.30	1.30±0.40	2.14±0.28
Scenario 6							
QCNet	33.65±4.52	27.86±10.28	90.52±15.58	48.55±12.74	11.91±2.35	N/A	N/A
GameFormer	57.82±18.64	70.98±34.60	65.00±22.43	22.35±6.29	17.52±2.06	N/A	N/A
MAPPO	7.01±1.21	5.69±0.79	27.21±0.82	5.30±0.82	3.13±0.61	N/A	N/A
TrafficGamer	0.72±0.53	1.09±0.56	1.39±1.33	1.49±0.66	0.63±0.34	N/A	N/A

Table 2: CCE-gap value at the last time step calculated using the Restricting Action Space method

Method	Agent 1	Agent 2	Agent 3	Agent 4	Agent 5	Agent 6	Agent 7
Scenario 1							
QCNet	16.00±5.13	5.32±2.50	9.67±3.23	22.31±3.70	13.92±0.51	N/A	N/A
GameFormer	21.85±2.51	11.27±6.19	15.48±5.21	85.46±15.52	28.83±7.31	N/A	N/A
MAPPO	14.70±1.68	4.95±0.55	8.99±1.11	7.16±0.96	10.22±1.18	N/A	N/A
TrafficGamer	13.17±1.30	3.56±1.06	6.33±1.41	8.34±0.88	8.77±0.96	N/A	N/A
Scenario 2							
QCNet	5.69±1.02	37.63±10.62	16.45±0.24	19.88±0.67	14.47±0.51	29.02±4.78	21.75±2.74
GameFormer	14.83±5.49	25.50±1.32	22.31±1.93	20.99±1.54	18.09±2.10	59.06±18.34	20.84 _{pm} 1.65
MAPPO	6.63±0.90	15.97±1.42	6.76±0.53	13.40±0.56	9.92±0.81	17.87±1.11	16.75±0.75
TrafficGamer	2.52±0.77	13.56±2.01	6.77±0.62	12.13±0.62	8.95±0.81	17.05±1.43	14.95±0.60
Scenario 3							
QCNet	18.84±3.83	9.31±1.40	8.47±5.26	12.96±3.71	4.36±0.83	1.55±0.49	6.40±0.77
GameFormer	51.65±16.59	18.75±5.53	18.14±10.20	53.29±16.05	19.67±9.20	21.49±8.76	23.66±5.94
MAPPO	13.22±0.84	3.58±1.51	8.50±0.51	15.78±0.73	0.65±0.16	1.20±0.78	7.58±0.82
TrafficGamer	11.73±1.13	3.68±1.40	9.04±0.87	4.20±1.58	0.86±0.26	1.65±0.56	5.01±0.63
Scenario 4							
QCNet	14.67±2.76	42.88±11.14	3.97±3.31	9.46±1.12	14.47±7.29	N/A	N/A
GameFormer	9.78±3.45	13.18±4.03	8.77±1.38	15.22±0.66	7.75±4.98	N/A	N/A
MAPPO	8.00±0.53	28.46±1.37	5.66±1.46	7.97±0.82	16.74±1.44	N/A	N/A
TrafficGamer	5.09±0.68	26.37±1.80	3.51±3.13	7.80±0.91	13.06±0.99	N/A	N/A
Scenario 5							
QCNet	5.22±1.85	14.60±8.33	7.94±0.48	2.79±0.91	13.64±4.75	21.03±0.60	10.02±0.43
GameFormer	13.92±5.96	48.58±17.36	17.50±5.18	23.06±10.27	8.42±2.09	25.75±0.81	11.48±1.09
MAPPO	2.67±0.46	20.33±2.47	3.02±0.44	3.42±0.51	6.07±0.54	15.39±0.36	2.83±0.36
TrafficGamer	3.33±0.62	13.09±1.73	2.85±0.50	2.03±0.65	4.49±1.16	12.83±0.37	1.94±0.38
Scenario 6							
QCNet	20.46±4.64	16.94±10.80	63.95±16.86	44.22±10.87	6.96±2.39	N/A	N/A
GameFormer	44.60±9.95	73.87±15.71	25.60±10.73	20.37±4.16	12.70±1.15	N/A	N/A
MAPPO	21.46±1.51	7.07±0.83	13.60±1.79	7.06±1.03	5.64±0.79	N/A	N/A
TrafficGamer	18.79±1.40	5.13±0.94	7.89±1.08	4.27±1.19	2.21±0.92	N/A	N/A